

# Melanoma addiction to the long non-coding RNA *SAMMSON*

Eleonora Leucci<sup>1,2</sup>, Roberto Vendramin<sup>1,2</sup>, Marco Spinazzi<sup>2</sup>, Patrick Laurette<sup>3</sup>, Mark Fiers<sup>2</sup>, Jasper Wouters<sup>4</sup>, Enrico Radaelli<sup>5</sup>, Sven Eyckerman<sup>6,7</sup>, Carina Leonelli<sup>8,9</sup>, Katrien Vanderheyden<sup>8,9</sup>, Aljosja Rogiers<sup>1,2</sup>, Els Hermans<sup>10</sup>, Pieter Baatsen<sup>2</sup>, Stein Aerts<sup>11</sup>, Frederic Amant<sup>10</sup>, Stefan Van Aelst<sup>12,13</sup>, Joost van den Oord<sup>4</sup>, Bart de Strooper<sup>2</sup>, Irwin Davidson<sup>3</sup>, Denis L. J. Lafontaine<sup>14</sup>, Kris Gevaert<sup>6,7</sup>, Jo Vandesompele<sup>8,9</sup>, Pieter Mestdagh<sup>8,9\*</sup> & Jean-Christophe Marine<sup>1,2\*</sup>

**Focal amplifications of chromosome 3p13–3p14 occur in about 10% of melanomas and are associated with a poor prognosis. The melanoma-specific oncogene *MITF* resides at the epicentre of this amplicon<sup>1</sup>. However, whether other loci present in this amplicon also contribute to melanomagenesis is unknown. Here we show that the recently annotated long non-coding RNA (lncRNA) gene *SAMMSON* is consistently co-gained with *MITF*. In addition, *SAMMSON* is a target of the lineage-specific transcription factor *SOX10* and its expression is detectable in more than 90% of human melanomas. Whereas exogenous *SAMMSON* increases the clonogenic potential in *trans*, *SAMMSON* knockdown drastically decreases the viability of melanoma cells irrespective of their transcriptional cell state and *BRAF*, *NRAS* or *TP53* mutational status. Moreover, *SAMMSON* targeting sensitizes melanoma to MAPK-targeting therapeutics both *in vitro* and in patient-derived xenograft models. Mechanistically, *SAMMSON* interacts with p32, a master regulator of mitochondrial homeostasis and metabolism, to increase its mitochondrial targeting and pro-oncogenic function. Our results indicate that silencing of the lineage addiction oncogene *SAMMSON* disrupts vital mitochondrial functions in a cancer-cell-specific manner; this silencing is therefore expected to deliver highly effective and tissue-restricted anti-melanoma therapeutic responses.**

*In silico* analysis of single nucleotide polymorphism (SNP) array data from >300 human clinical samples from The Cancer Genome Atlas (TCGA) revealed that the chromosome 3p melanoma-specific focal amplifications invariably encompass a recently annotated long intergenic non-coding RNA (lincRNA) gene, *SAMMSON*, which is located ~30 kilobase pair (kb) downstream of *MITF* (Fig. 1a and Extended Data Fig. 1a, b). Importantly, *SAMMSON* expression levels correlated with copy number gain ( $P < 0.001$ ; Fig. 1a). Genome-wide copy number analysis (CNA) of melanoma cell lines and short-term cultures (MM lines<sup>2</sup>) confirmed co-amplification of *MITF* and *SAMMSON* in a subset of these samples (Extended Data Fig. 1c).

Unexpectedly, although *MITF*-*SAMMSON* co-amplification only occurs in about 10% of melanomas, analysis of the TCGA RNA-sequencing (RNA-seq) data set detected *SAMMSON* in >90% of both primary and metastatic skin cutaneous melanomas (SKCMs; Fig. 1b and Extended Data Fig. 1a). *SAMMSON* was also detected in 16 out of 17 randomly selected MM lines (Extended Data Fig. 1d). MM001 was the only line that did not express *SAMMSON* owing to a decrease in copy number (Extended Data Fig. 1c, d). *SAMMSON* levels were comparable in cultures that exhibited a 'proliferative' and 'invasive' transcriptional

profile (Extended Data Fig. 1d)<sup>3</sup>. In contrast, *MITF*-M protein levels were high in the proliferative and low in the invasive cultures, respectively. Thus, the levels of *SAMMSON* and *MITF* do not strictly correlate. Likewise, there was no correlation between *SAMMSON* and *MITF* expression in the melanoma TCGA clinical samples (Extended Data Fig. 1e, f). Furthermore, there was no correlation between *SAMMSON* expression and any of the common melanoma somatic mutations such as *BRAF*, *NRAS* or *TP53* (data not shown).

While barely detectable, if at all, in normal human melanocytes (NHMEs) and in non-invasive melanoma lesions in the radial growth phase (RGP), *SAMMSON* expression was readily detectable in invasive vertical growth phase (VGP) samples (Fig. 1c). This indicates that *SAMMSON* expression is specifically induced as melanoma cells transit from an immortalized to a fully transformed cell state and is therefore a putative biomarker of melanoma malignancy.

Quantitative polymerase chain reaction with reverse transcription (RT-qPCR) analysis in 60 different cancer cell lines detected *SAMMSON* exclusively in the melanoma samples (Extended Data Fig. 1g, h). Analysis of RNA-seq data from a total of 8,085 tumour specimens from 24 cancer types (TCGA) confirmed selective expression in melanoma (Fig. 1d). Whereas *SAMMSON* expression was detectable in normal human melanoblasts, it was undetectable in NHME cultures and in normal adult tissues (Fig. 1e and data not shown).

Consistent with *SAMMSON* being a lincRNA, the expression of which is driven by its own promoter, a peak of H3K4me3 chromatin immunoprecipitation followed by sequencing (ChIP-seq) was detected upstream of its transcription start site (TSS) in melanoma cells (Fig. 1f). Similarly, a peak of H3K27ac, a marker of active enhancers and promoters, overlaps with the H3K4me3 peak at the *SAMMSON* promoter. H3K27ac peaks are also found upstream of *SAMMSON* in all but one (MM001) MM lines (Extended Data Fig. 2a). Consistent with the melanoma-specific expression of *SAMMSON*, such H3K27ac peaks could not be detected in the non-melanoma cancer cell lines profiled by ENCODE.

Interestingly, we identified putative *SOX*-binding sites upstream of the *SAMMSON* TSS. *SOX10* is a melanoblast/melanoma-specific transcription factor<sup>4</sup> and may therefore contribute to the melanoblast/melanoma-specific expression of *SAMMSON*. Consistently, *SOX10* and its co-factor *BRG1* (ref. 5), but not *MITF*, were recruited upstream of the *SAMMSON* TSS in melanoma cells (Fig. 1f, g and Extended Data Fig. 2b, c). Knockdown of *SOX10*, but not *MITF*, led to a decrease in *SAMMSON* expression (Fig. 1h and Extended Data Fig. 2d, e). These

<sup>1</sup>Laboratory For Molecular Cancer Biology, Center for Human Genetics, KULeuven, Herestraat 49, 3000 Leuven, Belgium. <sup>2</sup>Center for the Biology of Disease, VIB, Herestraat 49, 3000 Leuven, Belgium. <sup>3</sup>Institut de Génétique et de Biologie Moléculaire et Cellulaire (IGBMC), Rue Laurent Fries 1, 67404 Illkirch, France. <sup>4</sup>Laboratory of Translational Cell and Tissue Research, Department of Pathology, KULeuven and UZ Leuven, Herestraat 49, 3000 Leuven, Belgium. <sup>5</sup>Mouse Histopathology Core Facility, Center for the Biology of Disease, VIB-KULeuven, Herestraat 49, 3000 Leuven, Belgium. <sup>6</sup>Medical Biotechnology Center, VIB, Albert Baertsoenkaai 3, 9000 Gent, Belgium. <sup>7</sup>Department of Biochemistry, Gent University, Albert Baertsoenkaai 3, 9000 Gent, Belgium. <sup>8</sup>Center for Medical Genetics, Gent University, De Pintelaan 185, 9000 Gent, Belgium. <sup>9</sup>Cancer Research Institute Gent, Gent University, De Pintelaan 185, 9000 Gent, Belgium. <sup>10</sup>Gynaecologische Oncologie, KU Leuven, Herestraat 49, 3000 Leuven, Belgium. <sup>11</sup>Laboratory of Computational Biology, Center for Human Genetics, KULeuven, Herestraat 49, 3000 Leuven, Belgium. <sup>12</sup>Department of Applied Mathematics, Computer Science and Statistics, Gent University, De Pintelaan 185, 9000 Gent, Belgium. <sup>13</sup>Department of Mathematics, KU Leuven, Celestijnenlaan 200B, 3001 Leuven, Belgium. <sup>14</sup>RNA Molecular Biology, Center for Microscopy and Molecular Imaging, Université Libre de Bruxelles (ULB), rue des Professeurs Jeener et Brachet 12, 6041 Charleroi, Belgium.

\*These authors contributed equally to this work.

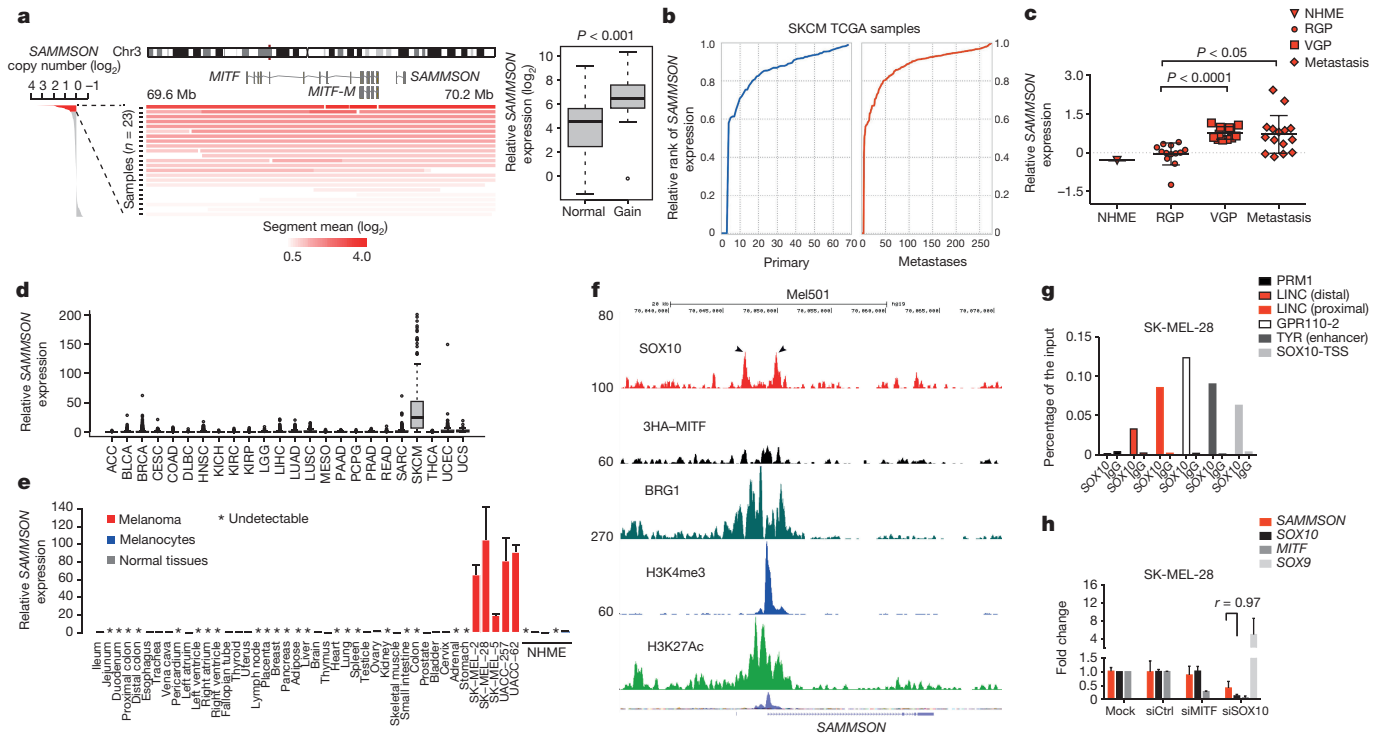


**Figure 1 | Gene amplification and SOX10-mediated transcription drives SAMMSON expression in melanoma.** **a**, DNA copy number of *SAMMSON* and *MITF* in melanoma lesions ( $n = 386$ ). Samples are ranked according to *SAMMSON* copy number, expressed as the mean log ratio of the segment encompassing *SAMMSON*. Samples with a *SAMMSON* log ratio  $> 0.5$  are shown (Mann–Whitney  $P < 0.001$ ). Chr, chromosome. **b**, Read counts were generated based on the GENCODE annotation (version 19) from the RNA-seq alignments of 345 SKCM samples (TCGA). 7,014 lncRNAs were selected for which the raw counts were normalized to reads per kb per million reads (RPKM) values. The rank expression of *SAMMSON* was determined, sorted and plotted for the primary (left) and metastatic (right) samples. **c**, Relative expression in NHME, RGP, VGP and metastatic melanoma. Significance was calculated by analysis of variance (ANOVA). **d**, Relative expression across a cohort of 8,085 primary tumour

samples from different cancer types. **e**, Relative expression across 38 adult tissues, 5 melanoma cell lines and NHME cultures. Error bars represent standard deviations (s.d.) of qPCR replicates ( $n = 2$ ). **f**, University of California, Santa Cruz (UCSC) Genome Browser screenshots of ChIP-seq data illustrating the selective recruitment of SOX10 to the *SAMMSON* loci and the co-localization of H3K4me3 and H3K27ac at the *SAMMSON* TSS in Mel501. **g**, ChIP-qPCR of SOX10 in SK-MEL-28 at the indicated loci. The IgG antibody was used as a negative control. **h**, Gene expression levels in untreated (Mock) SK-MEL-28 cells or cells transfected with a control siRNA pool (siCtrl) or pools targeting MITF (siMITF) or SOX10 (siSOX10). Data are an average of three biological replicates  $\pm$  standard error of the mean (s.e.m.).  $r$ , Pearson correlation coefficient.

data indicate that the lineage-specific expression profile of *SAMMSON* is a consequence of focal gene amplification and/or SOX10-mediated transcription.

Silencing *SAMMSON* using different locked nucleic acid (LNA)-modified antisense oligonucleotides (GapmeRs), which trigger RNase-H-mediated degradation of the target, greatly reduced the clonogenicity of all *SAMMSON*-expressing melanoma cultures independently of their *BRAF*, *NRAS* or *TP53* status (Fig. 2a, b and Extended Data Fig. 3a). The growth of ‘invasive’ melanoma cells (that is, MM165), and thereby intrinsically resistant to mitogen-activated protein kinase (MAPK) inhibitors<sup>3</sup> was also inhibited upon *SAMMSON* knockdown. Chronic treatment with inhibitors of BRAF(V600E) is invariably associated with the development of drug resistance<sup>6</sup>. Importantly, cells that acquired resistance to a BRAF(V600E) inhibitor (that is, SK-MEL-28-R) remained sensitive to *SAMMSON* targeting.

Compared with GapmeR11, GapmeR3 was more efficient in knocking down *SAMMSON* expression and had a greater growth inhibitory effect (Fig. 2a, b and Extended Data Fig. 3a, b). Although less efficient than GapmeR-mediated silencing, RNA interference (RNAi)-dependent knockdown of *SAMMSON* also inhibited melanoma growth (Extended Data Fig. 3c, d). In contrast, transfection of *SAMMSON*-targeting GapmeRs or short interfering RNA (siRNA) in MM001, NHME or non-melanoma cancer cell lines (that is, HCT116), all of which lack *SAMMSON*, did not cause growth inhibition (Fig. 2a, Extended Data Fig. 3b and data not shown). Moreover,

forced expression of *SAMMSON* and *SAMMSON* mutants, carrying mismatches into the GapmeR target sequences, efficiently rescued growth inhibition induced by GapmeR3/11 (Extended Data Fig. 3e). Importantly, the latter experiment also indicated that *SAMMSON* exerts its pro-survival function *in trans*.

Flow cytometry and Caspase-Glo 3/7 assays indicated that this growth inhibition is, at least partly, due to a significant induction of the intrinsic mitochondrial apoptotic pathway (Fig. 2c and Extended Data Fig. 3b). Exposure to an inhibitor of cytochrome-c-induced procaspase-9 activation rescued *SAMMSON* knockdown-mediated growth inhibition (Extended Data Fig. 3f).

Notably, ectopic expression of *SAMMSON* in MM001 cells conferred them with a growth advantage (Fig. 2d, e and Extended Data Fig. 3g, h), confirming that *SAMMSON* exerts its pro-oncogenic function *in trans*.

Overcoming intrinsic and acquired resistance to MAPK inhibitors requires the simultaneous targeting of multiple pathways. Interestingly, GapmeR3 enhanced the cytotoxic effects of the BRAF(V600E) inhibitor vemurafenib and MEK inhibitor pimasetib (Fig. 2f and Extended Data Fig. 3i).

Knockdown of *SAMMSON* did not decrease MITF levels (Extended Data Fig. 4), ruling out the possibility that *SAMMSON* promotes melanoma survival by enhancing *MITF* transcription *in cis*. Instead, consistent with a function *in trans*, *SAMMSON* primarily localizes to the cytoplasm, with a fraction co-localizing with mitochondria (Extended Data Figs 5 and 6).

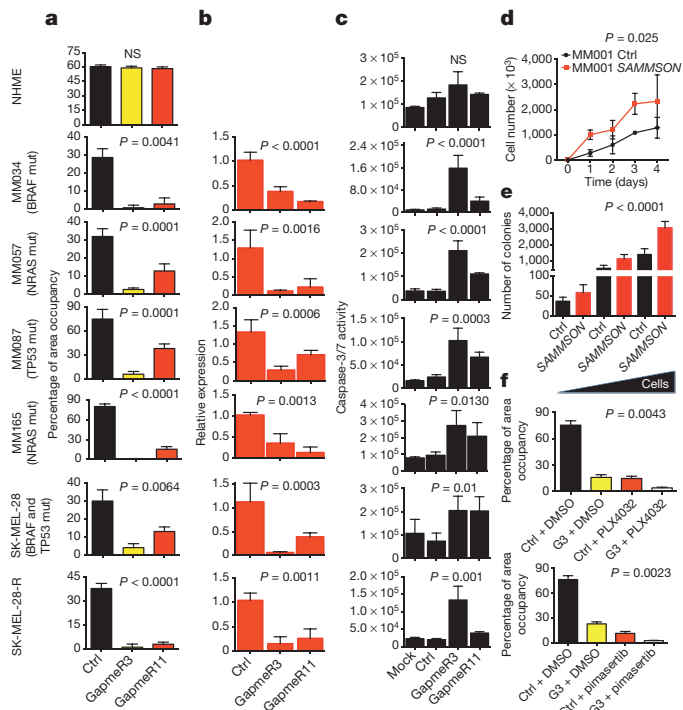


**Figure 2 | SAMMSON is required for melanoma growth and survival.** **a**, Quantification of colony formation assays 7 days after seeding of melanoma cells presented as the mean density (percentage of area occupancy) of three different biological replicates  $\pm$  s.e.m. *P* values were calculated by ANOVA. mut, mutation **b**, Relative SAMMSON expression in cells transfected with a GapmeR control (Ctrl), GapmeR3 and GapmeR11. The results are the average of three different biological replicates  $\pm$  s.e.m. *P* values were calculated by ANOVA. **c**, Caspase-Glo 3/7 assays in untreated cells (Mock) and cells transfected with GapmeR control (Ctrl), GapmeR3 and GapmeR11 (48 h post-transfection). The data are presented as the means of three different biological replicates  $\pm$  s.e.m. *P* values were calculated by ANOVA. NS, not significant. **d**, Cell proliferation assays in MM001 upon ectopic SAMMSON expression. **e**, Quantification of colony formation assays 7 days after seeding 1,000, 5,000 or 10,000 cells described in **d**. The data are presented as the mean number of colonies of three different biological replicates  $\pm$  s.e.m. at each density. *P* values were calculated by ANOVA. **f**, Quantification of colony formation assays 7 days after seeding of SK-MEL-28 cells transfected with a control GapmeR (Ctrl) or GapmeR3 and exposed to either vehicle or a half-maximum effective concentration ( $EC_{50}$ ) dose of vemurafenib (PLX4032) or pimasertib. The data are presented as the mean density of three different biological replicates  $\pm$  s.e.m. *P* values were calculated by ANOVA.

We next purified endogenous SAMMSON RNA complexes by adapting the RNA antisense purification–mass spectrometry (RAP–MS) and chromatin isolation by RNA purification (ChIRP)-like-MS methodologies<sup>7,8</sup>. After confirming that SAMMSON RNA, but not the housekeeping *TBC* and *UBC* messenger RNAs, was selectively retrieved (Fig. 3a), the SAMMSON-associated proteins were identified by mass spectrometry. Eighteen proteins were identified in multiple SAMMSON purifications from three independent biological samples (Extended Data Fig. 7a and Supplementary Tables 1, 2). The majority of these (12/18) are RNA-binding proteins, including XRN2, a protein involved in several key aspects of RNA metabolism. XRN2 was previously retrieved in ChIRP-MS experiments performed with different lncRNAs<sup>8</sup>, indicating that XRN2 may be a bona fide lncRNAs interactor.

Among the enriched proteins, p32 attracted our attention because of its established role in mitochondrial metabolism. In addition, p32 expression is elevated in cancers<sup>9–11</sup> and p32 knockdown decreases the growth of various cancer cell lines, including melanoma<sup>10,12</sup>. Consistently, p32 levels were elevated in the MM cultures compared with NHME cultures (Extended Data Fig. 7b, c). RAP followed by

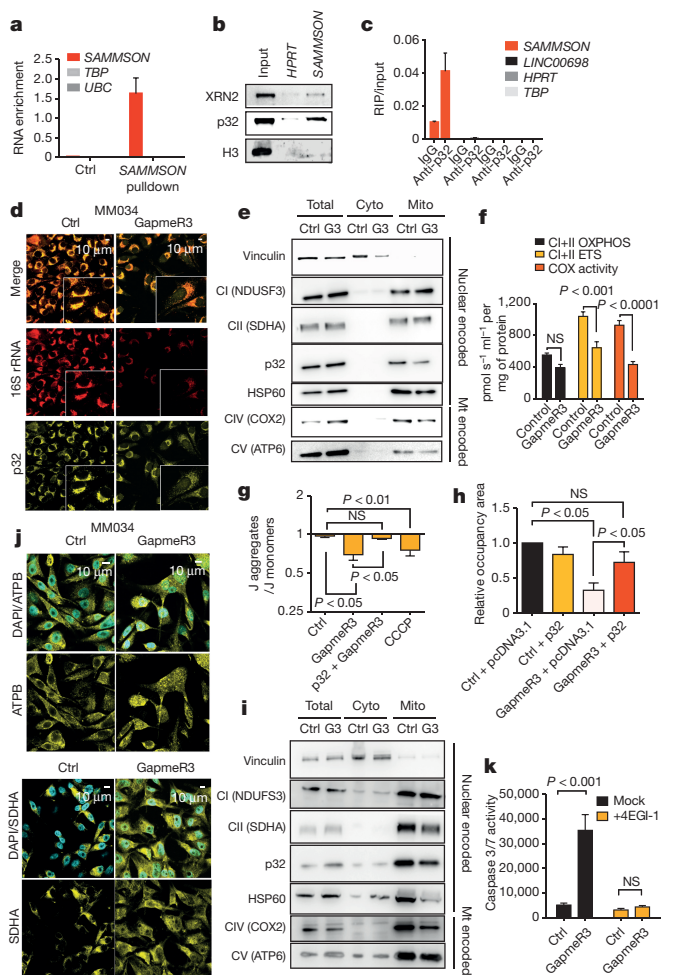


**Figure 3 | SAMMSON interacts with p32 to increase its mitochondrial localization and function.** **a**, SAMMSON (but not *TBP* or *UBC*) is specifically recovered by RAP. **b**, SAMMSON (and *HRPT*) pulldown after ultraviolet crosslinking and western blotting. **c**, SAMMSON is recovered by RIP using p32-specific antibodies. **d**, p32 immunofluorescence (yellow) and 16S rRNA fluorescence *in situ* hybridization (FISH; red) in MM034 cells transfected with a control GapmeR (Ctrl) or with GapmeR3. **e**, Western blotting 24 h after transfection of a control GapmeR (Ctrl) and GapmeR3 (G3). Cyto, cytosolic extracts; Mito, mitochondrial extracts; Mt encoded, mitochondria encoded. **f**, Measurement of the OXPHOS capacity (CI+II OXPHOS), electron transfer capacity of the respiratory chain (CI+II ETS) and COX activity using high-resolution respirometry of digitonin-permeabilized cells. Raw data were normalized to the total amount of proteins. The graph represents an average of four biological replicates  $\pm$  s.e.m. *P* values were calculated by ANOVA. NS, not significant. **g**, Mitochondrial membrane potential (JC-1) in SK-MEL-28 cells transfected with a control GapmeR (Ctrl) or with GapmeR3, and either with an empty or a p32-expressing vector. The graph shows an average of four different biological replicates  $\pm$  s.e.m. *P* values were calculated by ANOVA. **h**, Quantification of colony formation assays 5 days after seeding SK-MEL-28 cells transfected with a control GapmeR (Ctrl) or GapmeR3, and either with an empty or a p32-expressing vector. The data represent the occupancy area relative to Ctrl + pcDNA3.1. The data are an average of four biological replicates  $\pm$  s.e.m. *P* values were calculated by ANOVA. **i**, Western blotting analysis 33 h after transfection of a control GapmeR (Ctrl) and GapmeR3 (G3). **j**, Immunofluorescence for SDHA and ATP6B (and nuclear counterstaining using 4',6-diamidino-2-phenylindole (DAPI)) in MM034 cells transfected with a control GapmeR (Ctrl) or with GapmeR3. **k**, Caspase-Glo 3/7 activity (72 h post-transfection) in SK-MEL-28 cells transfected with a control GapmeR (Ctrl) or GapmeR3, and incubated (8 h post-transfection) with a CAP-dependent translation inhibitor (4EGI-1). The graph shows an average of three biological replicates  $\pm$  s.e.m. *P* value was calculated by ANOVA. **b**, **e**, **i**, For gel source data, see Supplementary Fig. 1.

western blotting analyses confirmed the association between p32 and SAMMSON. p32 was enriched in the SAMMSON pull-down relative to the samples bound to the negative control *HPRT* (Extended Data Fig. 7d). No enrichment was observed after purifications with either beads alone, in lysate pre-treated with RNase A, or using SAMMSON-null cells (Extended Data Fig. 7d and data not shown). To ensure that the interaction between SAMMSON and p32 is direct, we performed RAP followed by western blotting in cells in which covalent bonds between directly interacting RNA and proteins are created by ultraviolet crosslinking. p32 was still enriched in these conditions (Fig. 3b). We also performed RNA-immunoprecipitation (RIP) assays using p32-specific antibodies. Compared with the immunoglobulin G (IgG)-bound sample, all antibody-bound complexes showed a significant increase in the amount of SAMMSON RNA, but not of unrelated RNAs such as *HPRT*, *TBP* or *LINC00698* (Fig. 3c and Extended Data Fig. 7e).

Importantly, although no effect was seen on total p32 levels, a rapid decrease in its mitochondrial fraction, accompanied by an increase in nuclear targeting, was observed upon SAMMSON silencing (Fig. 3d, e and Extended Data Fig. 8a). p32 is required for the maturation of mitochondrial 16S rRNA, and thereby for the expression of mitochondrially encoded polypeptides, the maintenance of mitochondrial membrane potential and oxidative phosphorylation (OXPHOS)<sup>10,13–16</sup>. Consistently, the decrease in mitochondrial p32 was accompanied by reduced levels of 16S ribosomal RNA (Fig. 3d) and mitochondrial-DNA-encoded (COX2 and ATP6), but not nuclear-DNA-encoded (SDHA or NDUFS3), respiratory chain complex components (Fig. 3e). Moreover, the enzymatic activity of respiratory complexes I and IV, which contain proteins translated on mitochondrial ribosomes, was decreased upon SAMMSON silencing (Fig. 3f and Extended Data Fig. 8b). This decrease occurred before outer membrane permeabilization, as evidenced by the oxygraph profiles, and before induction of caspase-3/7 activity (data not shown).

The mitochondrial respiratory chain generates a proton gradient that establishes the mitochondrial membrane potential used to drive ATP production. A marked decrease in mitochondrial membrane potential was observed in SAMMSON-knockdown cells (Fig. 3g and Extended Data Fig. 8c), before the onset of apoptosis, accompanied by a slight, but significant, decrease in intracellular ATP levels (Extended Data Fig. 8d).

p32 controls mitochondrial homeostasis and integrity<sup>15,17,18</sup>. Accordingly, p32 silencing caused aberrant mitochondrial structures with fewer and fragmented cristae and reduced mitochondria matrix density. These effects were phenocopied upon SAMMSON knockdown (Extended Data Fig. 9).

Importantly, reintroduction of p32, but not of an N-terminally tagged version that can no longer be imported into the mitochondria, significantly rescued the SAMMSON-knockdown-dependent defect in mitochondrial membrane potential and growth inhibition (Fig. 3g, h and Extended Data Fig. 8e–g). SAMMSON silencing therefore inhibits melanoma survival at least partly by disrupting vital p32-mediated mitochondrial functions.

There is increasing evidence that mitochondrial translational deficiency induces a cytosolic stress response, which impairs cell growth<sup>19</sup>. This retrograde signalling is induced by the collapse of the mitochondrial membrane potential, which is critical for the import of nuclear-encoded proteins into the matrix<sup>20</sup>. This leads to the ‘toxic’ over-accumulation of mitochondrial precursors in the cytosol and activation of a stress response, which in yeast has been referred to as mitochondria precursor over-accumulation stress (mPOS)<sup>21,22</sup>. In turn, mPOS triggers cell cycle checkpoints and/or induces cell death depending on the cellular context. Interestingly, several hours after the collapse in the membrane potential, a decrease in the mitochondrial levels of several nuclear-encoded proteins (for example, SDHA, HSP60) was observed in SAMMSON-knockdown cells (Fig. 3i). Moreover, nuclear-encoded proteins such as SDHA and ATPB accumulated in the cytosol (and even in the nucleus for ATPB) of SAMMSON-knockdown cells (Fig. 3j and Extended Data Fig. 8h), indicating that SAMMSON

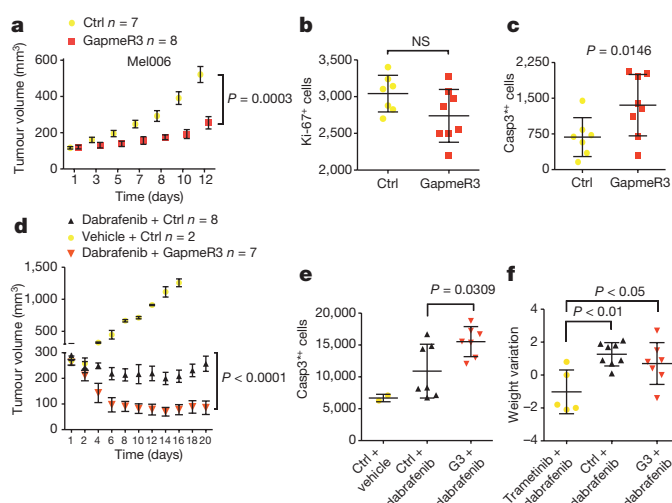


**Figure 4 | Therapeutic potential of SAMMSON targeting *in vivo*.**

**a**, Tumour volume of cohorts of Mel006 PDX mice treated (intravenous injections) with a control GapmeR (Ctrl) or GapmeR3. Data are the means  $\pm$  s.d. of different biological replicates ( $P$  value was calculated by two-ways ANOVA). **b**, **c**, Quantification of Ki-67-positive cells (**b**) and cleaved caspase 3-positive (Casp3<sup>+</sup>; **c**) of melanoma lesions treated as described in **a**.  $P$  value was calculated by *t*-test. NS, not significant. **d**, Tumour volume of cohorts of PDX mice (Mel006) treated with combinations of control GapmeR (Ctrl) and GapmeR3 with either vehicle or dabrafenib by daily oral gavage (vehicle or dabrafenib) and intravenous injection of the GapmeRs every 2 days. Data are means  $\pm$  s.d. of different biological replicates ( $P$  value was calculated by *t*-test). **e**, Quantification of cleaved caspase 3 of melanoma lesions treated as described in **d**. **f**, Weight variation of mice treated as described in **d** and mice exposed daily to dabrafenib and trametinib.  $P$  values were calculated by ANOVA.

silencing may lead to mitochondrial import defects, which, in turn, could activate mPOS.

In yeast, mPOS-induced cell death can be attenuated by reducing cytosolic protein translation, thus decreasing stress imposed by protein over-accumulation and aggregation<sup>21</sup>. Strikingly, exposure to a cap-dependent translation inhibitor significantly rescued SAMMSON-knockdown-induced apoptotic cell death (Fig. 3k). Notably, consistent with data indicating that mitochondrial translation stress may engage the p53 pathway<sup>23</sup>, SAMMSON silencing triggered a significant p53 response in several melanoma cultures (data not shown). However, p53 knockdown did not rescue caspase-3/7 induction and growth inhibition, indicating that p53 is not strictly required for SAMMSON-knockdown-induced growth inhibition.

To test the therapeutic potential of SAMMSON targeting *in vivo*, we used two patient-derived xenograft (PDX) melanoma models (Mel006 and Mel010; Extended Data Fig. 10a). Intravenous treatment with the SAMMSON-targeting GapmeR3 significantly suppressed the growth of Mel006 tumours, decreased cell proliferation and increased apoptosis (Fig. 4a–c). Gene expression profiles of the GapmeR3-treated melanoma lesions showed enrichment for signatures associated with decreased cell proliferation, activation of p53 and decreased OXPHOS, mitochondrial ribosome biogenesis and respiratory chain complex activity (Extended Data Fig. 10b). Notably, this treatment did not cause any relevant adverse reaction or weight loss (data not shown). Tumour growth was also inhibited upon intra-tumour injections of GapmeR3 into Mel010 tumours (Extended Data Fig. 10c).

Importantly, whereas tumour growth was only inhibited after exposure to the BRAF(V600E) inhibitor dabrafenib alone, tumour regression and a significant increase in apoptosis were observed upon exposure to both dabrafenib and GapmeR3 (Fig. 4d, e and Extended Data Fig. 10d). Notably, these mice did not suffer from any relevant adverse events or weight loss, in contrast to mice treated with a combination of dabrafenib and MEK inhibitor (trametinib; Fig. 4f).

The observation that some cancer cells are dependent on OXPHOS for survival led to the development of agents that exploit bioenergetics and metabolic alterations in mitochondria<sup>24</sup>. The use of such agents is, however, complicated by their dangerous side effects. We show here that *SAMMSON* is a lineage-specific lincRNA that promotes melanoma survival through its ability to enhance the mitochondrial localization and function of p32, a protein required for the maintenance of OXPHOS<sup>10</sup>. Given that *SAMMSON* is expressed specifically in the vast majority (>90%) of melanomas, but not in normal adult tissues, these data identify *SAMMSON* as an attractive therapeutic target for the disruption of mitochondrial metabolism selectively in melanoma.

*MITF*, which is co-amplified with *SAMMSON* in a subset of melanomas, also promotes mitochondrial respiration by inducing PGC-1 $\alpha$  (refs 25, 26). The *MITF-SAMMSON* amplicon therefore favours oxidative metabolism via two distinct mechanisms, the *MITF-PGC-1 $\alpha$*  axis and the *SAMMSON-p32* axis, making these cells particularly OXPHOS dependent.

Treatment of melanoma with BRAF inhibitors induces the *MITF-PGC-1 $\alpha$* -dependent oxidative metabolic program and renders them highly dependent on OXPHOS<sup>26</sup>. This observation explains why co-targeting of *SAMMSON* and mutant BRAF promotes potent anti-tumour responses. *SAMMSON* targeting may therefore offer a novel therapeutic avenue to overcome the adaptive metabolic reprogramming that limits the efficacy of BRAF inhibitors. Moreover, as melanoma cells that acquire resistance to BRAF inhibitors remain addicted to *SAMMSON* expression, *SAMMSON* targeting might be a valid therapeutic approach to treat relapsed patients.

In addition, *MITF*-low invasive cells, although glycolytic, remain addicted to *SAMMSON* expression. These cells may still be dependent on mitochondria for functions other than ATP generation, such as fatty acid synthesis and glutaminolysis<sup>27,28</sup>. Interestingly, p32 has recently been shown to be required for MYC-induced addiction<sup>11</sup>. Through its ability to modulate mitochondrial protein synthesis, *SAMMSON* is also likely to affect processes outside the mitochondrion<sup>19</sup>. Consistently, we provide evidence that *SAMMSON* targeting decreases melanoma survival in an mPOS-dependent manner.

These findings warrant further investigation about the potential of *SAMMSON* as an informative biomarker of malignancy and as a highly selective and broad-spectrum anti-melanoma therapeutic target. Given the recent surge in optimism about antisense drugs, this therapeutic approach may be rapidly applicable to the clinic.

**Online Content** Methods, along with any additional Extended Data display items and Source Data, are available in the online version of the paper; references unique to these sections appear only in the online paper.

Received 21 December 2015; accepted 21 January 2016.

- Garraway, L. A. *et al.* Integrative genomic analyses identify *MITF* as a lineage survival oncogene amplified in malignant melanoma. *Nature* **436**, 117–122 (2005).
- Gembarska, A. *et al.* *MDM4* is a key therapeutic target in cutaneous melanoma. *Nature Med.* **18**, 1239–1247 (2012).
- Verfaillie, A. *et al.* Decoding the regulatory landscape of melanoma reveals TEADS as regulators of the invasive cell state. *Nature Commun.* **6**, 6683 (2015).
- Harris, M. L., Baxter, L. L., Loftus, S. K. & Pavan, W. J. Sox proteins in melanocyte development and melanoma. *Pigment Cell Melanoma Res.* **23**, 496–513 (2010).
- Laurette, P. *et al.* Transcription factor *MITF* and remodeler *BRG1* define chromatin organisation at regulatory elements in melanoma cells. *eLife* **4**, 06857 (2015).
- Flaherty, K. T. *et al.* Inhibition of mutated, activated *BRAF* in metastatic melanoma. *N. Engl. J. Med.* **363**, 809–819 (2010).
- McHugh, C. A. *et al.* The *Xist* lincRNA interacts directly with *SHARP* to silence transcription through *HDAC3*. *Nature* **521**, 232–236 (2015).
- Chu, C. *et al.* Systematic discovery of *Xist* RNA binding proteins. *Cell* **161**, 404–416 (2015).
- Amamoto, R. *et al.* Mitochondrial p32/C1QBP is highly expressed in prostate cancer and is associated with shorter prostate-specific antigen relapse time after radical prostatectomy. *Cancer Sci.* **102**, 639–647 (2011).
- Fogal, V. *et al.* Mitochondrial p32 protein is a critical regulator of tumor metabolism via maintenance of oxidative phosphorylation. *Mol. Cell. Biol.* **30**, 1303–1318 (2010).

- Fogal, V. *et al.* Mitochondrial p32 is upregulated in Myc expressing brain cancers and mediates glutamine addiction. *Oncotarget* **6**, 1157–1170 (2015).
- Fogal, V., Zhang, L., Krajewski, S. & Ruoslahti, E. Mitochondrial/cell-surface protein p32/gC1qR as a molecular target in tumor cells and tumor stroma. *Cancer Res.* **68**, 7210–7218 (2008).
- Muta, T., Kang, D., Kitajima, S., Fujiwara, T. & Hamasaki, N. p32 protein, a splicing factor 2-associated protein, is localized in mitochondrial matrix and is functionally important in maintaining oxidative phosphorylation. *J. Biol. Chem.* **272**, 24363–24370 (1997).
- Yagi, M. *et al.* p32/gC1qR is indispensable for fetal development and mitochondrial translation: importance of its RNA-binding ability. *Nucleic Acids Res.* **40**, 9717–9737 (2012).
- Hu, M. *et al.* p32 protein levels are integral to mitochondrial and endoplasmic reticulum morphology, cell metabolism and survival. *Biochem. J.* **453**, 381–391 (2013).
- Matos, P. *et al.* A role for the mitochondrial-associated protein p32 in regulation of trophoblast proliferation. *Mol. Hum. Reprod.* **20**, 745–755 (2014).
- Li, Y., Wan, O. W., Xie, W. & Chung, K. K. K. p32 regulates mitochondrial morphology and dynamics through parkin. *Neuroscience* **199**, 346–358 (2011).
- Jiao, H. *et al.* Chaperone-like protein p32 regulates *ULK1* stability and autophagy. *Cell Death Differ.* **22**, 1812–1823 (2015).
- Richter-Dennerlein, R., Dennerlein, S. & Rehling, P. Integrating mitochondrial translation into the cellular context. *Nature Rev. Mol. Cell Biol.* **16**, 586–592 (2015).
- Chacinska, A., Koehler, C. M., Milenkovic, D., Lithgow, T. & Pfanner, N. Importing mitochondrial proteins: machineries and mechanisms. *Cell* **138**, 628–644 (2009).
- Wang, X. & Chen, X. J. A cytosolic network suppressing mitochondria-mediated proteostatic stress and cell death. *Nature* **524**, 481–484 (2015).
- Wrobel, L. *et al.* Mistargeted mitochondrial proteins activate a proteostatic response in the cytosol. *Nature* **524**, 485–488 (2015).
- Richter, U. *et al.* A mitochondrial ribosomal and RNA decay pathway blocks cell proliferation. *Curr. Biol.* **23**, 535–541 (2013).
- Fantin, V. R. & Leder, P. Mitochondriotoxic compounds for cancer therapy. *Oncogene* **25**, 4787–4797 (2006).
- Vazquez, F. *et al.* PGC1 $\alpha$  expression defines a subset of human melanoma tumors with increased mitochondrial capacity and resistance to oxidative stress. *Cancer Cell* **23**, 287–301 (2013).
- Haq, R. *et al.* Oncogenic *BRAF* regulates oxidative metabolism via PGC1 $\alpha$  and *MITF*. *Cancer Cell* **23**, 302–315 (2013).
- Wise, D. R. & Thompson, C. B. Glutamine addiction: a new therapeutic target in cancer. *Trends Biochem. Sci.* **35**, 427–433 (2010).
- Dang, C. V. Links between metabolism and cancer. *Genes Dev.* **26**, 877–890 (2012).

**Supplementary Information** is available in the online version of the paper.

**Acknowledgements** GapmeRs were designed by J. Lai. This work was supported by the Fonds Wetenschappelijk Onderzoek (FWO; #G.0646.14N and #3G056613), Foundation Against Cancer (STK#2014-126), UGent-IOF (F2013/IOF-Advanced/676) and STK grant F/2014/376. The PDX studies were funded by GOA/14/012 (KULeuven) and KPC\_29\_005 (Belgian Ministries of Health). The authors wish to thank N. Samyn for help with MS, M. Van Gele for providing NHME cultures and P. Wolter for scientific discussions and his central role in the establishment of the melanoma PDX platform. E.L. is a recipient of a postdoctoral fellowship from the Marie-Curie/VIB OMICS program. M.S. is the recipient of EMBO fellowship (ALTF 648-2013). F.A. is a senior researcher from the Research Fund Flanders (FWO). P.M. and R.V. are recipients of FWO postdoctoral and PhD fellowships, respectively. D.L. is supported by the Fonds National de la Recherche (FRS/FNRS). I.D. is supported by the Institut National du Cancer PAIR melanoma (MELA13-002), the “France Génomique” consortium (ANR10-INBS-09-08), and ANR-10-LABX-0030-INRT. The I.D. laboratory is an “équipe labellisée Ligue Nationale contre le Cancer”.

**Author Contributions** E.L. and R.V. performed most experiments. M.S. performed the experiments described in Fig.3f. P.L., S.A. and I.D. provided ChIP-seq data. J.W. and J.v.d.O. provided melanoma clinical samples. J.v.d.O. and E.R. provided histopathology support. S.E. and K.G. performed the mass spectrometric measurement and analysis. C.L., K.V., S.V.A. and P.M. performed copy number variant analysis and profiling experiments and interpretation of the data. A.R., E.H. and F.A. provided support with the PDX models. P.B. provided technical support for the electron microscopy. P.M., M.F. and S.A. provided bioinformatics support. D.L.J.L., B.d.S., P.M. and J.V. helped with the interpretation of the data. J.-C.M. and E.L. designed most of the experiments and wrote the manuscript.

**Author Information** Mass spectrometry data have been deposited in the Proteomics Identifications Database under accession numbers PXD002565. Gene expression data have been deposited in the Gene Expression Omnibus under accession number GSE70180. Reprints and permissions information is available at [www.nature.com/reprints](http://www.nature.com/reprints). The authors declare no competing financial interests. Readers are welcome to comment on the online version of the paper. Correspondence and requests for materials should be addressed to J.-C.M. (JeanChristophe.Marine@cme.vib-kuleuven.be).

## METHODS

**Cell culture.** The melanoma cell lines Mel501, SK-MEL-28 (obtained from ATCC) were grown in 5% CO<sub>2</sub> at 37 °C in RPMI 1640-glutamax (Gibco, Invitrogen) or DMEM (for Mel501) supplemented with 10% FBS (Hyclone, Thermo Fisher Scientific). Sequences of the GapmeRs and siRNAs are indicated later.

Caspase 9 inhibitor was purchased from Merck Millipore (218761). 4EGI-1 was purchased from Selleckchem and used at a final concentration of 10 μM. The patient-derived low-passage MM cell lines (a gift from the Ghanem laboratory) were grown in F-10 (Gibco, Invitrogen), supplemented with 10% FBS (Hyclone, Thermo Fisher Scientific) and 12 mM glutamine.

NHMEs were grown in MGM-4 melanocyte growth medium (Lonza). Cells were transfected by Lipofectamine 2000 according to manufacturer instructions with 25 nM of GapmeR (Exiqon). For siRNA experiments the cells were transfected with 25–50 nM siRNAs or Dharmacon Pools and harvested 24 and/or 48 h after transfection. All cell lines used in this study were mycoplasma negative.

**Human melanoma samples.** Early stages of melanoma from the UZ Leuven archive were isolated by laser capture microdissection and RNA extracted with Arcturus PicoPure Frozen RNA Isolation Kit (Life Technologies).

**RAP-MS.** For affinity purification of SAMMSON protein targets, 100 μg of Streptavidin Sepharose High Performance (GE Healthcare) was coupled to 400 pmol of biotinylated probes against SAMMSON (Biosearch Technologies) overnight at 4 °C. Cells (60 × 10<sup>6</sup> cells per sample) were lysed in 2 ml of pull-out buffer (20 mM Tris-HCl, pH 7.5, 200 mM NaCl, 2.5 mM MgCl<sub>2</sub>, 0.05% Igepal, 60 U Superase-In per ml (Ambion), 1 mM dithiothreitol (DTT) and a cocktail of protease inhibitors) and incubated for 3 h with the beads at 4 °C. As a negative control, an additional sample was digested with 10 μg ml<sup>-1</sup> RNase A digestion for 10 min at room temperature before incubation with SAMMSON probes.

For the crosslinking experiments, cells were washed once in PBS, crosslinked dry at 400 mJ cm<sup>-2</sup> and lysed. During the washes the amount of Triton X-100 was doubled and SDS was added to a final concentration of 0.02%.

For mass spectrometry, samples were processed by a short separation on SDS-PAGE gels (Biorad) to remove contaminants possibly interfering with downstream analysis. After excision, washing and drying of the gel band, digestion buffer (50 mM NH<sub>4</sub>HCO<sub>3</sub>, 5 μg ml<sup>-1</sup> trypsin) was added to fully submerge the dried gel band, and the sample was digested for 16 h at 37 °C. The generated peptide mixtures were acidified, dried and re-dissolved in a 2% CH<sub>3</sub>CN (acetonitrile), 0.1% formic acid solution.

The obtained peptide mixtures were introduced into a liquid chromatography-tandem mass spectrometry (LC-MS/MS) system through an ultimate 3000 RSLC nano LC (Thermo Scientific) inline connected to a Q Exactive mass spectrometer (Thermo Fisher Scientific). The sample mixture was first loaded on a trapping column (made in house, 100 μm internal diameter (i.d.) × 20 mm, 5 μm beads C18 Reprosil-HD, Dr. Maisch, Ammerbuch-Entringen). After flushing from the trapping column, the sample was loaded on an analytical column (made in house, 75 μm i.d. × 150 mm, 5 μm beads C18 Reprosil-HD, Dr. Maisch) packed in the nanospray needle (PicoFrit SELF/P PicoTip emitter, PF360-75-15-N-5, NewObjective). Peptides were loaded with loading solvent (0.1% TFA in water) and separated with a linear gradient from 98% solvent A' (0.1% formic acid in water) to 40% solvent B' (0.08% formic acid in water/acetonitrile, 20/80 (v/v)) in 30 min at a flow rate of 300 nl min<sup>-1</sup>. This was followed by a 15 min wash reaching 99% solvent B'. The mass spectrometer was operated in data-dependent, positive ionization mode, automatically switching between MS and MS/MS acquisition for the 10 most abundant peaks in a given MS spectrum.

The source voltage was 3.4 kV, and the capillary temperature was 275 °C. One MS1 scan (*m/z* 400–2,000, AGC target 3 × 10<sup>6</sup> ions, maximum ion injection time 80 ms) acquired at a resolution of 70,000 (at 200 *m/z*) was followed by up to 10 tandem MS scans (resolution 17,500 at 200 *m/z*) of the most intense ions fulfilling the defined selection criteria (AGC target 5 × 10<sup>4</sup> ions, maximum ion injection time 60 ms, isolation window 2 Da, fixed first mass 140 *m/z*, spectrum data type: centroid, underfill ratio 2%, intensity threshold 1.7 × 10<sup>4</sup>, exclusion of unassigned, 1, 5–8, and >8 charged precursors, peptide match preferred, exclude isotopes on, dynamic exclusion time 20 s). The HCD collision energy was set to 25% normalized collision energy and the polydimethylcyclosiloxane background ions at 445.120025 Da were used for internal calibration (lock mass).

From the MS/MS data in each LC run, Mascot Generic Files were created using Distiller software (version 2.4.3.3, Matrix Science, <http://www.matrixscience.com/distiller.html>). While generating these peak lists, grouping of spectra was allowed in Distiller with a maximal intermediate retention time of 30 s and a maximal intermediate scan count of 5 was used where possible. Grouping was done with 0.005 Da precursor ion tolerance. A peak list was only generated when the MS/MS spectrum contains more than 10 peaks. There was no de-isotoping and the relative signal to noise limit was set at 2. These peak lists were then searched using

the Mascot search engine (MatrixScience)<sup>29</sup> with the Mascot Daemon interface (version 2.4.1, Matrix Science). Spectra were searched against the human protein entries in the Swiss-Prot database (SP2014\_07; 20284 sequence entries). Variable modifications were set as methionine oxidation, pyro-glutamate formation of N-terminal glutamine, propionamide formation on cysteine and acetylation of the protein N terminus. The mass tolerance on precursor ions was set to 10 ppm (with Mascot's C13 option set to 1) and on fragment ions to 20 mmu. The instrument setting was put on ESI-QUAD. Enzyme was set to trypsin, allowing for one missed cleavage. Only peptides that were ranked first and scored above the threshold score, set at 99% confidence, were withheld. The protein candidates that were pursued in this work were consistently identified with at least two different peptides in the relevant conditions (no peptides detected in the bead controls).

**RIP.** RIP was performed as previously described<sup>7</sup>. p32 and XRN2 were immunoprecipitated using 4 μg of specific antibody (Bethyl laboratories) coupled to 50 μl of protein G Dynabeads (Invitrogen) for 3 h.

**Cellular fractionation.** Briefly, total nuclear and cytoplasmic extracts were isolated from 20-cm ø dishes using Nuclei EZ prep (Sigma-Aldrich) according to the manufacturer's instructions. RT-qPCR for *MALAT1* and *TBP* were used to assess the purity of the fractions.

Mitochondria were purified from 20-cm ø dishes using mitochondria isolation kit for cultured cells (Thermo Fisher Scientific). Mitochondria enrichment was validated by western blot using antibodies directed against mitochondrial proteins (that is, ATPB). Mitoplasts were obtained by incubating mitochondria in hypotonic buffer (HEPES pH 7.2) for 20 min on ice.

**Antibodies.** Western blotting experiments were performed using the following primary antibodies: vinculin (V9131, Sigma-Aldrich, 1:10,000), histone 3 (ab1791, Abcam, 1:1,000), GAPDH (ab9485, Abcam, 1:1,000), p32 (A302-863A, Bethyl Laboratories, 1:5,000), XRN2 (A301-103A, Bethyl Laboratories, 1:2,000), SOX10 (N-20, Santa Cruz, 1:500), MITF (ab12039, Abcam, 1:1,000) and SDHA (Abcam AB14715, 1:1,000), COX2 (molecular probes A6404, 1:10,000), HSP60 (BD 611562, 1:5,000), NDUFS3 (Abcam 14711, 1:1,000), ATP6 (Abcam 192423, 1:1,000).

**Cell growth and cell death assays.** To detect cell death, cells were stained for 15 min with annexin V and PI using the FITC Annexin V Apoptosis Detection Kit II (BD Biosciences) according to the manufacturer's instructions. Cell death was detected on a MACSQuant VYB (Miltenyi Biotec BV) and data were analysed with FlowJo software (Tree Star).

Caspase 3 and 7 activity was measured using Caspase-Glo 3/7 luciferase assay (Promega) and VICTOR X4 Reader (PerkinElmer) 48 and 72 h after transfection of GapmeRs.

**Colony assay and cell count.** Cells were plated in six-well plates at the appropriate density and cultured for 1 week. The cells were washed with PBS, fixed and stained for 15 min with a 1% crystal violet in 35% methanol solution.

For vital counts, cells were stained with Trypan Blue (Sigma-Aldrich) and counted with TC20 automated cell counter (Biorad).

BRAF and MEK inhibitors (vemurafenib and pisetimab) were used at a concentration of 5 and 1 μM, respectively.

**SAMMSON cloning, mutagenesis and lentiviral transduction.** SAMMSON was synthesized by GenScript and cloned into pPGK (Addgene) lentiviral vector. Lentivirus produced in HEK293 cells were used to infect the MM001 cells. Successfully infected cells were selected in puromycin (0.5 μg ml<sup>-1</sup>)-containing medium for 1 week.

**Pharmacological treatment of mice.** The Mel0010 and Mel006 PDX models derived from two different metastatic melanoma lesions, both carrying the BRAF(V600E) mutation. Written informed consent was obtained from both patients and all procedures involving human samples were approved by the UZ Leuven/KU Leuven Medical Ethical Committee (# ML8713/S54185). All procedures involving animals (NMRI nude, 4-week-old females) were performed in accordance with the guidelines of the Catholic University of Leuven (KU Leuven) Animal Care and Use Ethical Committee (P147/2012).

Once tumours reached 150 mm<sup>3</sup>, 10 mg kg<sup>-1</sup> of GapmeR3 or control GapmeR were injected i.v. or directly into the tumours every 2 days for up to 20 days. For combination therapy with BRAF inhibitor, cohorts of Mel006 were enrolled into the experiment once tumours reached 250 mm<sup>3</sup> in volume. Dabrafenib or vehicles were administered daily by oral gavage. The GapmeRs, at a concentration of 10 mg kg<sup>-1</sup>, were administered i.v. every 2 days.

No specific randomization method was used. According to animal welfare guidelines, mice have to be killed when tumours reach a volume of 2,000 mm<sup>3</sup> or when their body weight decreases more than 20% from the initial weight. Mice used in this paper never reached or overcame these limits. The investigators were blinded for the evaluation of the results.

**FISH for SAMMSON.** For detection of SAMMSON at a single-cell level, a pool of 48 FISH probes was designed using the Stellaris probe designer software (Biosearch

Technologies). Cells were grown on slides and fixed in 3.7% formaldehyde and permeabilized in ethanol 70%. Hybridization was carried out overnight at 37°C in 2× SSC, 10% formamide and 10% dextran. Cells were counterstained with DAPI and visualized using an Olympus Fluoview FV1200 using a LD635 laser for Cy5, LD559 HeNe for Cy3.5 and LD405 for DAPI.

**Electron microscopy.** Cells were fixed with 2.0% paraformaldehyde/2.5% EM-grade glutaraldehyde in 0.1 M sodium cacodylate buffer (pH 7.4) at 37°C overnight and collected. After fixation, samples were placed in 1% osmium tetroxide for 2 h and dehydrated in a graded series of ethyl alcohol. The agar-embedded samples were cut with a Leica UCT ultramicrotome in 50–70 nm sections and imaged in a JEOL JEM1400 transmission electron microscope at 80 kV.

**Immunohistochemistry and immunofluorescence.** Tumour biopsies formalin-fixed and paraffin embedded from the UZ Leuven archives, were cut in sections of about 4 μm. Samples were deparaffinized and dehydrated with xylene and graded alcohols, and subsequently rehydrated with demineralized water. Specimens were stained with haematoxylin and eosin and immunohistochemistry was performed using microwave pre-treatment of slides for antigen retrieval. Antibodies against Ki-67 (SP6, Thermo Fisher Scientific #RM-9106-S, clone SP6, 1:200) and cleaved caspase 3 (Asp175, Cell Signaling Technology, 1:300) were applied, in conjunction with goat anti-rabbit horseradish peroxidase (HRP)-conjugated antibodies (DAKO) and visualized by DAB reaction. To evaluate the stainings, positive cells in the blue channel were counted in four different fields using ImageJ. Statistical significance was calculated by two-way ANOVA.

For immunofluorescence, cells were grown on slides and permeabilized in Triton X-100-containing buffer. Blocking was performed in 5% BSA and 10% goat serum. To detect p32 a rabbit antibody from Bethyl Laboratories was used 1:1,000 followed by staining with an anti-rabbit AlexaFluor-488 (Life Technologies, 1:500). Images were analysed on an Olympus fluoview FW1200 using a LD635 laser for Cy5, LD559 HeNe for Cy3.5 and LD405 for DAPI. To detect ATPB (AB14730) and SDHA (ab66484) antibodies from Abcam were used according to the manufacturer's instructions.

**RT-qPCR lncRNA expression profiling.** Expression of 1,718 lncRNAs was measured on the NCI60 cell line panel using the SmartChip Human lncRNA1 panel (Wafergen Biosystems). NCI60 cell lines were obtained through the Developmental Therapeutics Program (National Cancer Institute (NCI)). Previously misclassified cell lines NCI/ADR-RES and MDA-MB-435 were correctly annotated in the analysis. RNA was isolated using the miRNeasy mini kit (Qiagen) and reverse transcribed (2 μg) using the iScript Advanced RT kit (Bio-Rad) according to the manufacturer's instructions. A qPCR reaction mixture containing 2 μg of cDNA and SsoAdvanced Universal SYBR Green mastermix was dispensed using the MultiSample NanoDispenser across the 5,184-nanowell SmartChip and analysed using the SmartChip Cycler (Wafergen Biosystems). lncRNA expression was measured in triplicate and median Cq values were normalized using the global mean normalization strategy<sup>30</sup>. RNA from normal adult tissues (Ambion and Biochain) and primary melanocytes was reverse transcribed using the iScript RT kit (Bio-Rad). *SAMMSON* expression was measured by qPCR on a LightCycler 480 (Roche) and normalized in qbase+ (Biogazelle) using *HPRT1*, *TBP* and *SDHA* as reference genes.

**Microarray gene expression profiling.** Protein-coding gene expression in xenografts was measured using a custom gene expression microarray (SurePrint 8 × 60k, Agilent) or commercial microarray (SurePrint G3 Human Gene Expression v.2, Agilent) respectively. RNA (100 ng) was labelled using the Quick Amp polyA labelling kit and hybridized according to the manufacturer's instructions. Slides were scanned using a high-resolution microarray scanner (Agilent) and probe intensities were extracted using Feature Extraction software (Agilent). Signals were background corrected and Quantile normalized using the limma package in R. Only those probes expressed twofold above the mean signal of a negative control probe were retained for further analysis.

**Differential gene expression and pathway analysis.** Probes were collapsed to gene level by retaining the probe with the highest average signal across all samples. Probes expressed in less than half of the samples were discarded for differential gene expression analysis. Genes differentially expressed across four cell lines (SK-MEL-28, MM034, MM057, MM087) upon knockdown of *SAMMSON* were identified using the limma package with cell line as a blocking variable. For differential expression analysis in xenograft tumours, no blocking variable was applied. Genes with an adjusted *P* value < 0.05 and twofold expression change were selected as differentially expressed. Gene set enrichment analysis was performed on mRNA lists, pre-ranked according to the limma *t*-statistic using all curated gene sets from the Molecular Signatures Database.

**Generalized additive models.** Protein-coding gene expression data for the NCI60 cohort were obtained from the Developmental Therapeutics Program (NCI) data portal. Expression of each of the 1,718 lncRNAs (response variable) was analysed

in relation to cancer type and transcription factor expression (predictor variables) using generalized additive models (GAMs). A total of 1,270 transcription factors were analysed. GAMs were constructed using the mgcv package in R using the following parameters: family = "Gaussian", link = "identity", method = "GCV.Cp". The GAM value for each model represents the percentage of lncRNA expression variance explained by the predictor variable.

**Quantification of RNA-FISH data.** Tiff Z-stacks were imported using the StarSearch software package for automated spot counting of defined regions. Nuclear and total cell spots were counted for MM057, MM087 and SK-MEL-28 cells. Nuclear lncRNA copy number was defined as the average number of nuclear spots while cytoplasmic lncRNA copy number was defined as the difference between the number of total cell spots and the number of nuclear spots.

**Analysis of expression and copy number data from the TCGA cohort.** Level 3 segmented DNA SNP array data for 386 melanoma tumours was obtained through the TCGA data portal. *SAMMSON* copy number was defined as the mean log ratio of the overlapping segment(s). Expression data for *SAMMSON* (uc003dog) and *SOX10* (uc003aun) in melanoma and 23 additional cancer types were extracted from level 3 TCGA RNA-seq data, totalling 8,085 primary tumour samples.

***SAMMSON* transcript boundaries.** The *SAMMSON* TSS site was identified by means of CAGE-seq tags in two melanoma cell lines obtained from the FANTOM5 study (<http://fantom.gsc.riken.jp/5/>). The *SAMMSON* 3' end was identified by means of 3' RACE. Briefly, an anchored oligo-dT primer (AATACGACTCACTATAGGCGCTTTTTTTTTTTTTTTTTTTTTTTTTV) was used for cDNA synthesis of SK-MEL-28 RNA using the iScript select reverse transcription kit (BioRad). The 3' end was amplified (forward: AGCCAAATTTCAATGA GCCCCT; reverse: AATACGACTCACTATAGGC GC) and the resulting PCR amplicon was sized using the labchip (Calliper). The 3' end was identified based on the amplicon length and location of the forward primer.

**High-resolution respirometry.** SK-MEL-28 cells were resuspended in 20 mM HEPES, 110 mM sucrose, 10 mM KH<sub>2</sub>PO<sub>4</sub>, 20 mM taurine, 60 mM lactobionic acid, 3 mM MgCl<sub>2</sub>, 0.5 EGTA, pH 7.1, 1 mg ml<sup>-1</sup> fatty-acid-free BSA and catalase 280 U ml<sup>-1</sup>. Mitochondrial oxygen consumption was measured after plasma membrane permeabilization with digitonin 10 μg ml<sup>-1</sup> in an Oroboros 2k apparatus at 37°C. The oxygen consumption rates, expressed as pmol O<sub>2</sub> s<sup>-1</sup> mg protein<sup>-1</sup>, were measured after addition of the following substrates and specific inhibitors. (1) 2.5 mM pyruvate, 1 mM malate, 10 mM glutamate in the absence of ADP to determine complex-I-driven non phosphorylating respiration (CI leak). (2) 2.5 mM ADP to determine complex-I-driven phosphorylating respiration (CI OXPHOS). The coupling efficiency between oxygen consumption and phosphorylation was estimated as the ratio between CI OXPHOS and CI leak. (3) 10 mM succinate to determine the phosphorylating oxygen consumption driven by simultaneous activation of complex I and II (CI+II OXPHOS). (4) Titrating concentrations of the mitochondrial uncoupler CCCP to reach the maximal, uncoupled respiration (CI+II electron transfer system). (5) 0.5 μg ml<sup>-1</sup> antimycin A to block mitochondrial respiration at the level of complex III, and estimate residual non-mitochondrial oxygen consumption. (6) 2 mM ascorbate, 0.5 mM TMPD to measure cytochrome *c* oxidase (CIV)-driven respiration. (7) 10 μg ml<sup>-1</sup> cytochrome *c* to evaluate mitochondrial outer membrane damage. (8) 250 μM potassium cyanide to measure residual chemical background. CIV-driven respiration was measured as the cyanide sensitive oxygen consumption.

**Measurement of ATP production, mitochondrial membrane potential and ROS production.** Luciferase-based measurement of ATP production was obtained using Molecular Probes kit according to the manufacturer's instructions.

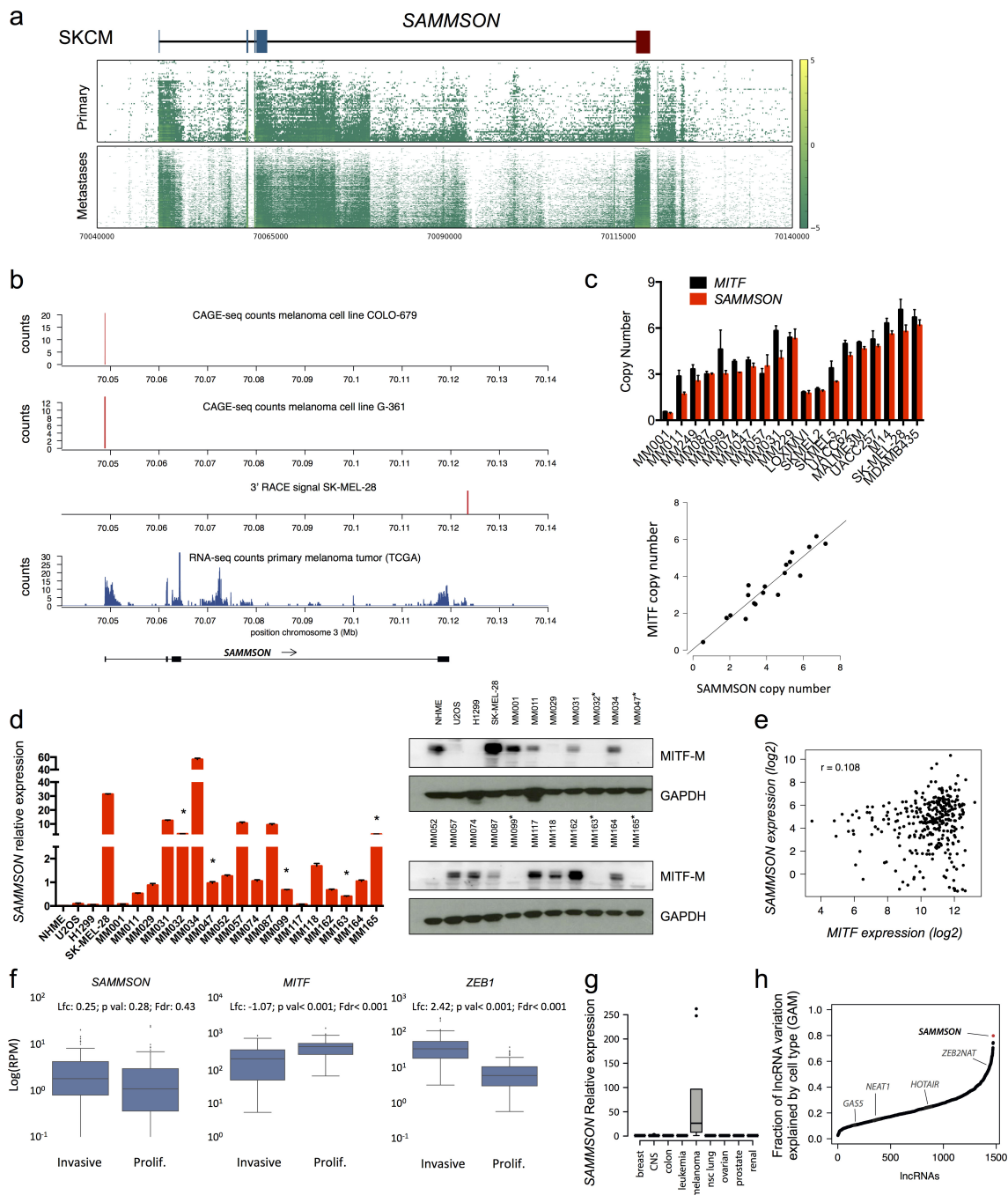
Mitochondrial membrane potential was measured by flow cytometry on a MACSQuant VYB (Miltenyi Biotec BV) using JC-1 dye (Molecular Probes). Data were analysed with FlowJo software (Tree Star) and the extent of depolarization was defined by the ratio between J-aggregates and J-monomers.

**Primers and siRNAs used.** *HPRT* forward, AGCCAGACTTTGTTGGA TTTG; reverse, TTTACTGGCGATGTCAATAAG; *TBP* forward, CGGC TGTTAACTTCGCTTC; reverse, CACACGCCAAGAAACAGTGA; *UBC* forward, ATTTGGGTCGCGGTTCTTG; reverse, TGCCTTGACATT CTCGATGGT; *MITF-M* forward, CATTGTTATGCTGGAAAGTACAGAA; reverse, GGCTTGCTGTATGTGGTACTTGG; *SOX10* forward, TACCCGC ACCTGCACAAC; reverse, TTCAGCAGCCTCCAGAGC; *SOX9* forward, GCAAGCTCTGGAGACTTCTG; reverse, GTACTTGTAATCCGGGTGGTC; *p32* forward, ACACCGACGGAGACAAAG; reverse, GGGATGCTGTTG TTAATGTTG; *MALAT1* forward, GGATCCAGGAAGGAGCGAG; reverse, ATTGCCGACCTCACGGATTT; *SAMMSON* forward, TTCCTCAACTATGCAACTCAA; reverse, TAGACTACGGGCTCATGACTT; *SAMMSON* forward #2, CCTCTAGATGTGTAAGGGTAGT; reverse #2, TTGAGTTGCATAGTTGAGGAA; *GPR110* forward, CAGTATTG

TGGCGGAAAAGC; reverse, CATCTTGCATGGCCCCA; TYR forward, AGCAGGCTCAGTCGATACAG; reverse, CACTGGGAATGAAGGGCAAG; SAMMSON GapmeR3, GTGTGAACTGGCT; GapmeR11, TTTGAGAG TTGGAGGA; non-targeting GapmeR; TCATACTATATGACAG; sip32.1 sense, GGTGAAGAACAGGAGCCT; antisense, AGGCTCCTGTTCTTC AACC; sip32.2 sense, TCACGGTCACTTTCAACAT; antisense, ATGTTG AAAGTGACCGTGA; SAMMSON siRNA sense, GUCGCUAGACAUU

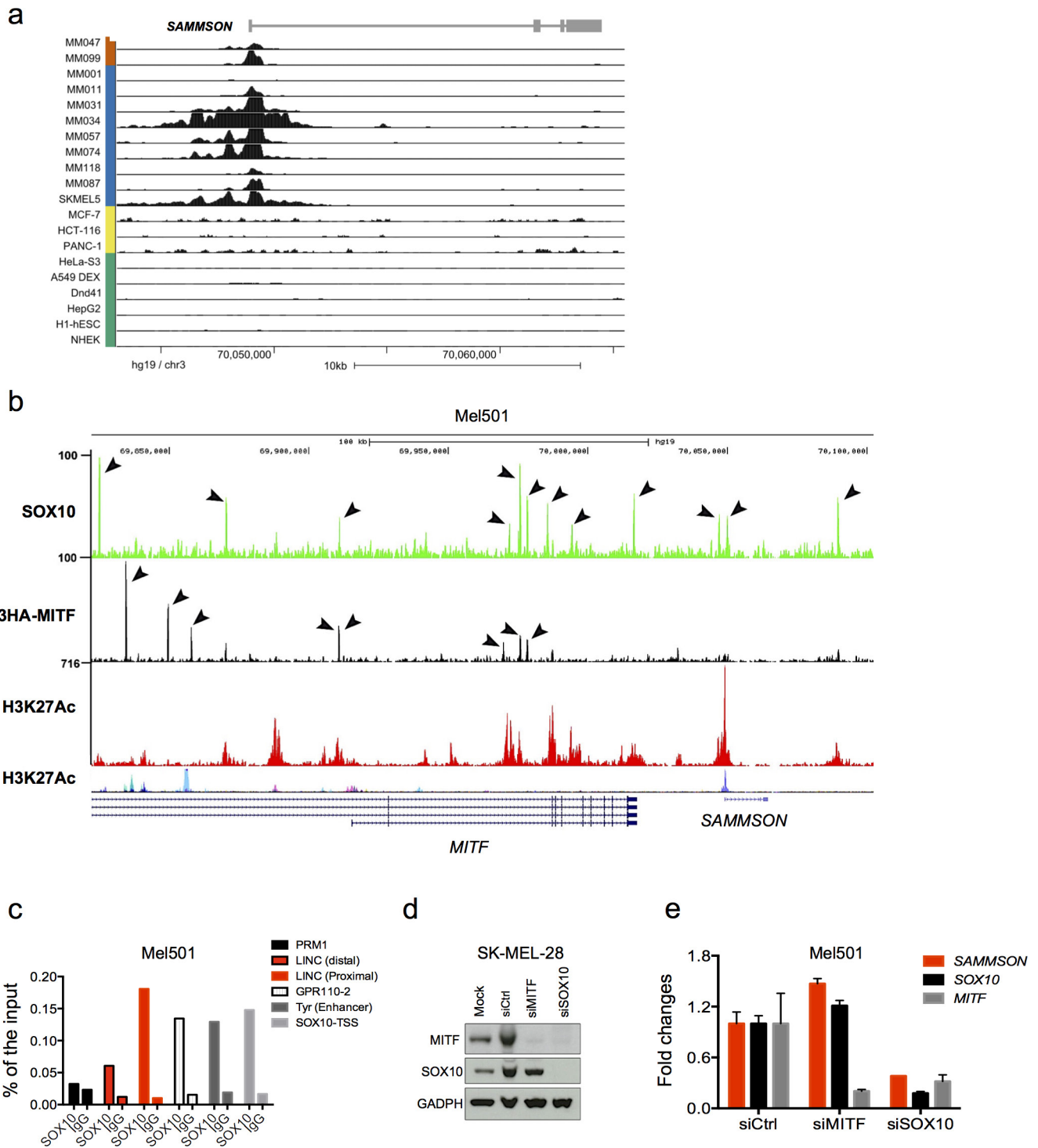
UGAGGA[dA][dA]; siRNA antisense UCCUCAAUGUCUAGCGAC[dA] [dA]; SOX10 and MITF knockdown, Dharmacon Smartpool.

29. Perkins, D. N., Pappin, D. J., Creasy, D. M. & Cottrell, J. S. Probability-based protein identification by searching sequence databases using mass spectrometry data. *Electrophoresis* **20**, 3551–3567 (1999).
30. Mestdagh, P. *et al.* A novel and universal method for microRNA RT–qPCR data normalization. *Genome Biol.* **10**, R64 (2009).



**Extended Data Figure 1 | SAMMSON is a lineage-specific lncRNA expressed in the vast majority of melanomas.** **a**, SAMMSON is a polyadenylated and multi-exonic lncRNA that contains one additional exon (in red) downstream of the four GENCODE19-annotated exons (blue). For each melanoma (SKCM) sample in the TCGA, the mapped RNA-seq data were converted into a coverage plot. The coverage data are normalized for library size and log<sub>1p</sub> transformed. Subsequently, the coverage data for all primary (SKCM.01) and metastatic samples (SKCM.06) in the region chromosome 3:70,040,000–70,140,000 is plotted as two heat maps. **b**, Cap analysis of gene expression-sequencing (CAGE-seq), RNA-seq data and RT-qPCR analyses from short-term melanoma cultures (MM lines) confirmed that SAMMSON is not a read-through transcript from the upstream MITF locus. CAGE-seq counts as defined by the FANTOM5 mammalian promoter expression atlas for two melanoma cell lines at the SAMMSON locus (panels 1 and 2), location of the 3' rapid amplification of cloned/cDNA ends (RACE) fragment for SAMMSON (panel 3) and RNA-seq counts from a primary melanoma tumour in the SAMMSON locus. **c**, SAMMSON and MITF copy number as measured by qPCR in short-term melanoma cultures and melanoma cell

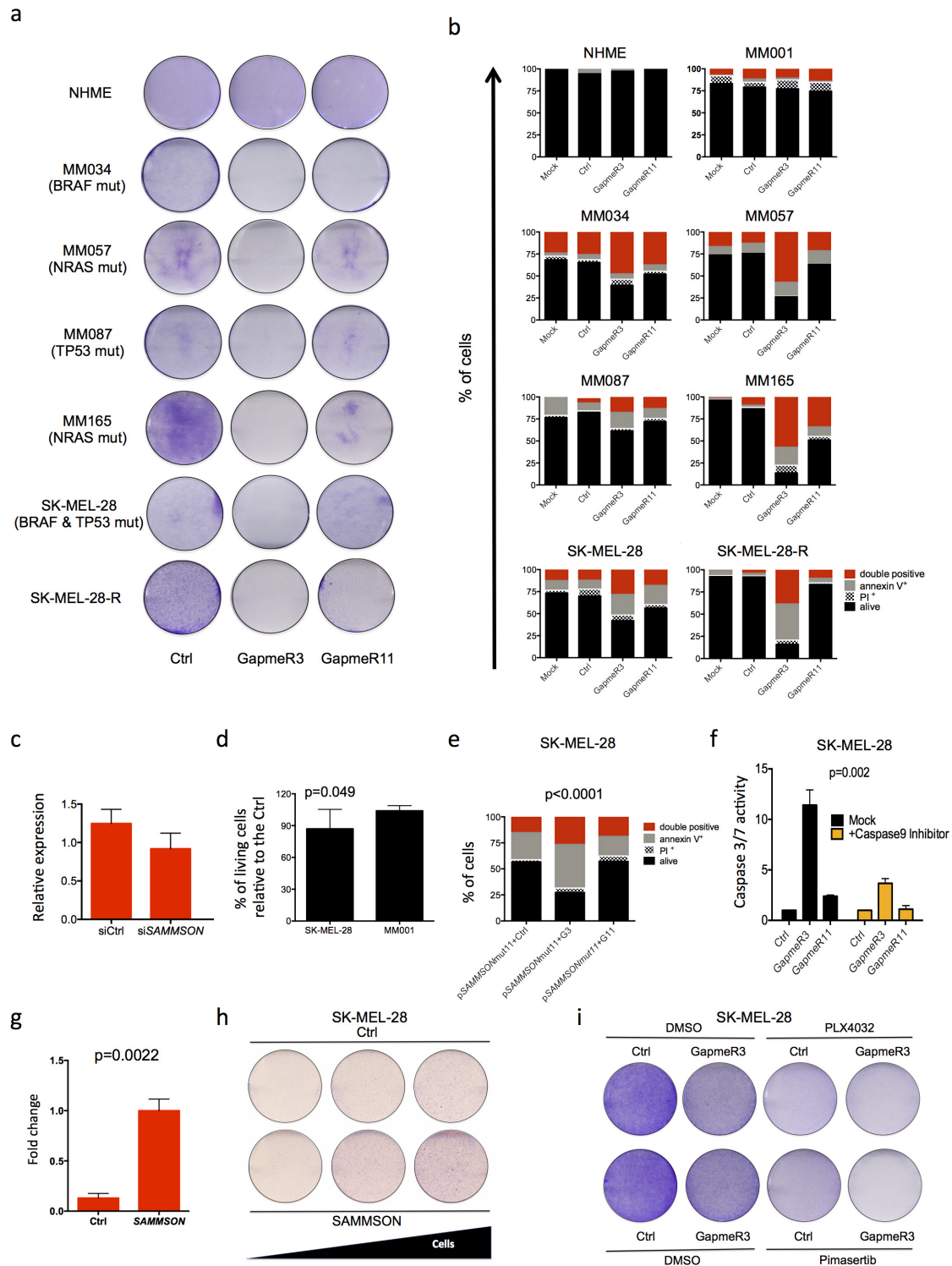
lines. Reference human genomic DNA was used as scaling control. Error bars represent s.d. of qPCR replicates ( $n = 2$ ). A significant correlation between MITF and SAMMSON copy number was observed (bottom; Spearman's rank  $\rho = 0.933$ ,  $P < 0.001$ ). **d**, Expression of SAMMSON in human short-term melanoma (MM) and NHME cultures relative to the expression average of three housekeeping genes (left) and correlation with MITF expression by western blot (right; for gel source data, see Supplementary Fig. 1). Error bars represent s.d. of three replicates ( $n = 3$ ). **e**, Expression correlation between MITF-M and SAMMSON in melanoma clinical samples from the TCGA database. **f**, Read counts were generated from RNA-seq data from TCGA melanoma samples (SKCM) and normalized to the library size. Samples were subdivided into proliferative and invasive groups as described previously<sup>3</sup> and box plots were generated for SAMMSON, ZEB1 and MITF. Differential expression analysis between the proliferative and invasive groups was done using edgeR50. lfc, log fold change; pval, uncorrected  $P$  value; fdr, false-discovery-rate-corrected pval. **g**, Relative expression in 60 cancer cell lines (NCI60 panel). **h**, Fraction of lncRNA expression variation ( $n = 1,472$ ) across the NCI60 panel by cancer type according to a generalized additive model (GAM).



**Extended Data Figure 2 | SAMMSON expression in melanoma, but not other cancer, cell lines, is at least partly SOX10-dependent.**

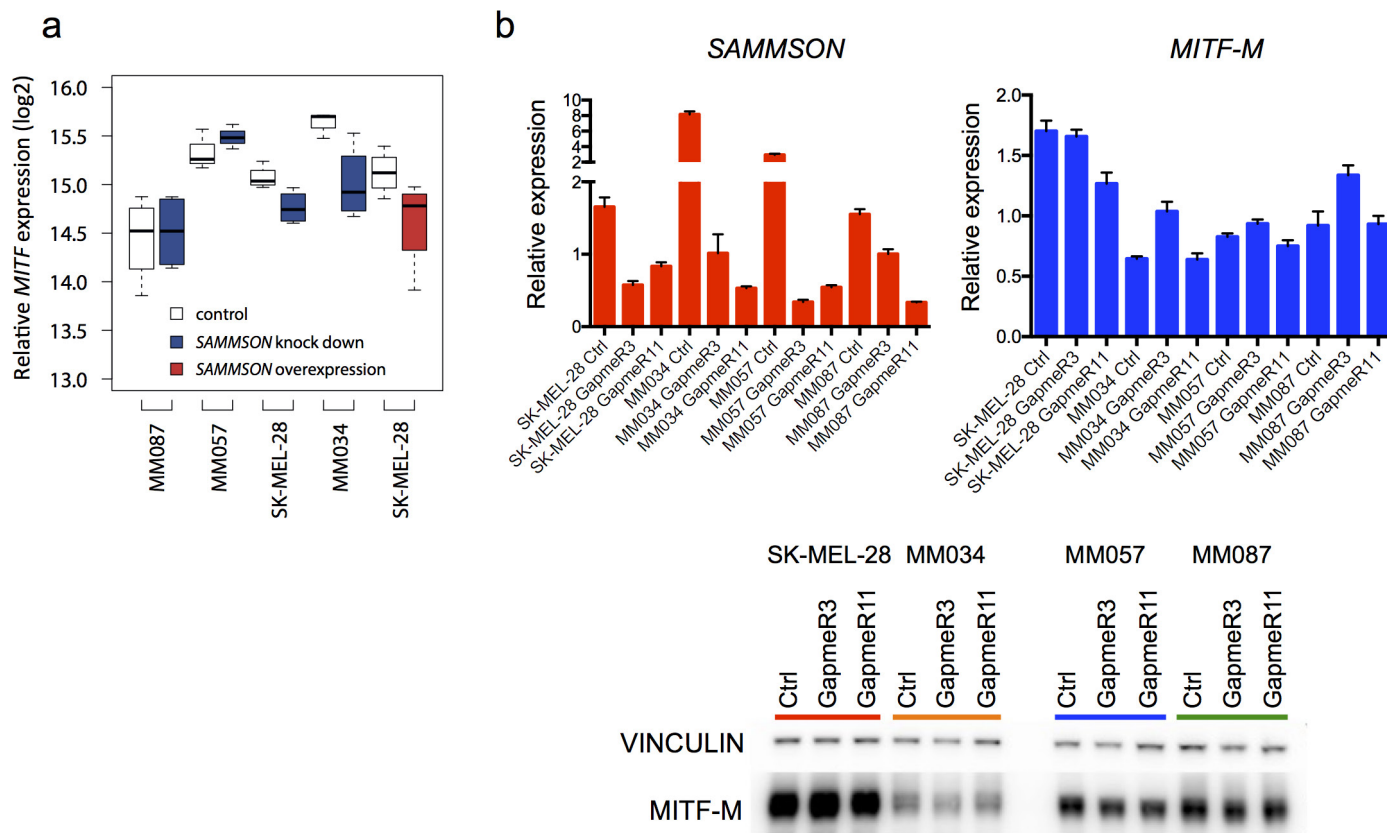
**a**, H3K27ac ChIP-seq data generated in house using a series of short-term melanoma cultures<sup>2</sup> were integrated with cancer cell lines data retrieved from ENCODE. A clear H3K27ac peak is present upstream SAMMSON in all, but one (MM001), melanoma lines. No peak is detected in the vast majority (19/20) of non-melanoma cancer cell lines, of which 9 are shown. **b**, UCSC screenshots of ChIP-seq data for SOX10, 3HA-MITF and H3K27ac at the MITF and SAMMSON loci in Mel501. **c**, ChIP-qPCR of

endogenous SOX10 in 501Mel cells at the indicated loci. The IgG antibody was used as a negative control. SOX10 recruitment to its well-established targets *GPR110*, *TYR* and *SOX10* itself, but not to a non-SOX10 target *PRM1*, confirms the specificity of the SOX10 ChIP experiment. **c**, Western blotting analysis of total protein lysates of SK-MEL-28 confirming efficient knockdown of SOX10 and MITF. GAPDH was used as a loading control (for gel source data, see Supplementary Fig. 1). **e**, Fold change RNA expression levels in 501Mel cells transfected with a control siRNA pool (siCtrl) or pools targeting MITF (siMITF) or SOX10 (siSOX10).



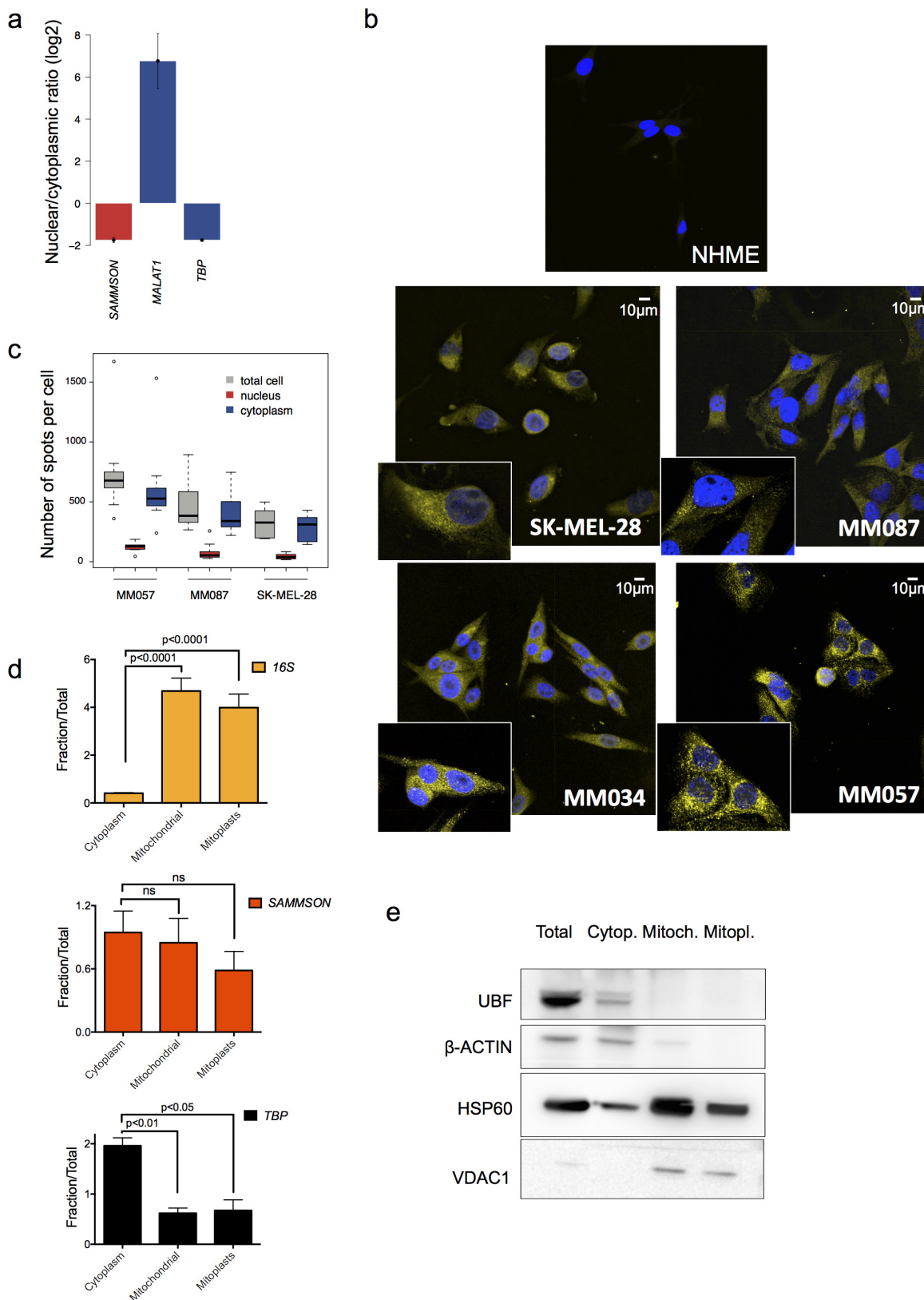
**Extended Data Figure 3 | SAMMSON promotes the *in vitro* growth and survival of human melanomas.** **a**, Colony formation assays 7 days after seeding of metastatic melanoma cells transfected with a GapmeR control (Ctrl), GapmeR3 and GapmeR11. **b**, Evaluation of cell death by co-staining for annexin V and propidium iodide (PI) followed by flow cytometric analysis. The graph is an average of three biological replicas and shows the percentage of cells alive, single positive or double positive. **c**, Efficiency of SAMMSON knockdown using an siRNA against SAMMSON. The expression of SAMMSON is relative to the average of three different housekeeping genes. **d**, Percentage of remaining living cells upon siSAMMSON, measured by flow cytometry, is indicated on y-axis  $\pm$  s.e.m. **e**, Evaluation of the capacity of exogenous SAMMSON and SAMMSON mutants (SAMMSONgap3mut and SAMMSONgap11mut, in which mismatches were introduced into the GapmeR3 and GapmeR11

target sequences) to rescue cell death in SK-MEL-28 treated with GapmeRs. The percentage of remaining living cells is indicated on the y-axis  $\pm$  s.e.m. **f**, Effect of a caspase-9 inhibitor on caspase-3/7 activation in SK-MEL-28 treated with GapmeRs. The graph is an average of three biological replicas; caspase-3/7 activity is relative to control sample (Ctrl)  $\pm$  s.e.m. *P* value was calculated by ANOVA. **g**, Relative SAMMSON expression in MM001 cells transfected with an empty or SAMMSON-encoding expression vector of three different biological replicas  $\pm$  s.e.m. *P* values were calculated by ANOVA. **h**, Colony formation assays 7 days after seeding 1,000, 5,000 or 10,000 MM001 as described in **g**. **i**, Colony formation assays 7 days after seeding of SK-MEL-28 transfected with a control GapmeR (Ctrl) or GapmeR3 and exposed to either vehicle or an EC<sub>50</sub> dose of vemurafenib (PLX4032) or pimasertib.



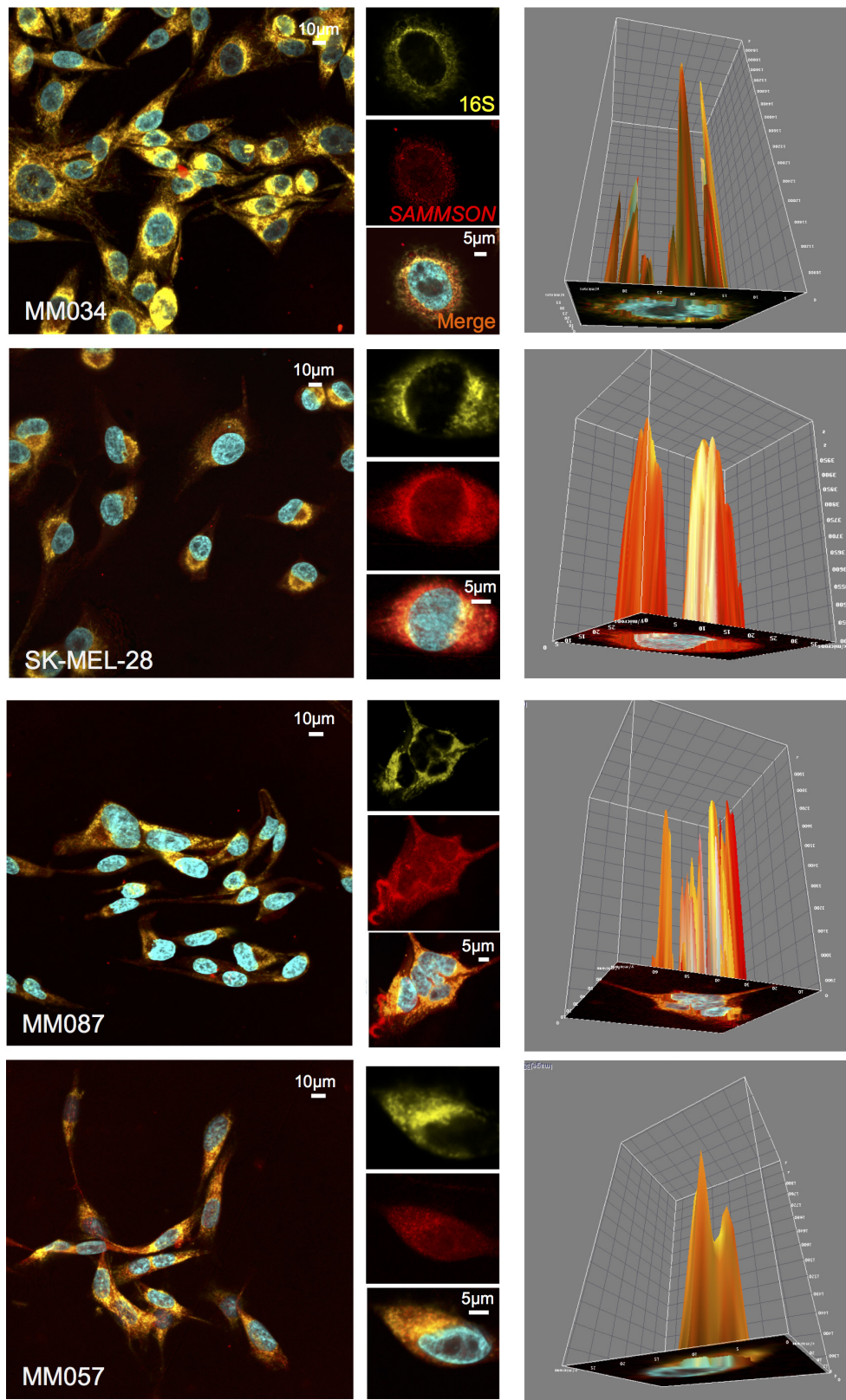
**Extended Data Figure 4 | *SAMMSON* does not regulate *MITF* expression in cis.** **a**, Relative expression of *MITF* as determined by microarray gene expression profiling in the indicated melanoma cell lines treated with GapmeR3 (*SAMMSON* knockdown) ( $n > 3$ ) or expressing exogenous *SAMMSON* ( $n = 4$ ); no significant differences in *MITF* expression were observed (limma, Benjamini-Hochberg adjusted  $P > 0.05$ ), except in MM034, in which *SAMMSON* knockdown resulted

in a 1.5-fold downregulation of *MITF* (limma, Benjamini-Hochberg adjusted  $P = 0.013$ ). **b**, Validation of the array data in **a** by qPCR for *SAMMSON* (left) and *MITF-M* (right) in all the cell lines used for the arrays. Expression is relative to three different housekeeping genes. The graph shows an average of three different biological replicas  $\pm$  s.e.m. The *MITF-M* protein levels were assessed by western blotting (bottom; for gel source data, see Supplementary Fig. 1).



**Extended Data Figure 5 | a**, SAMMSON localizes primarily to the cytoplasm and largely co-localizes with mitochondria. Quantification of SAMMSON in nuclei and cytoplasm of SK-MEL-28. Data are expressed as nuclear/cytoplasmic ratio  $\pm$  s.e.m. Data are shown for MALAT1 (exclusively nuclear) and TBP (cytoplasmic). The graph shows an average of three different fractionation experiments. **b**, SAMMSON RNA-FISH in a panel of melanoma cell lines and NHMEs. SAMMSON is shown in yellow and DAPI in blue. **c**, Quantification of SAMMSON RNA-FISH results described in **b**. Number of fluorescent spots in total per cell, nucleus

and cytoplasm of MM057 ( $n = 10$ ), MM087 ( $n = 10$ ) and SK-MEL-28 ( $n = 7$ ) melanoma cells are shown. **d**, Quantification of SAMMSON in cytoplasm, mitochondria and mitoplasts of SK-MEL-28. Data are expressed as fraction/total ratio  $\pm$  s.e.m. Data are shown for mitochondrial 16S rRNA (exclusively mitochondrial) and TBP (cytoplasmic). The graph is an average of three different fractionation experiments. **e**, The purity of the fractions was assessed by western blotting using nuclear (UBF1), cytoplasmic ( $\beta$ -actin) and mitochondrial markers (HSP60 and VDAC1; for gel source data, see Supplementary Fig. 1).

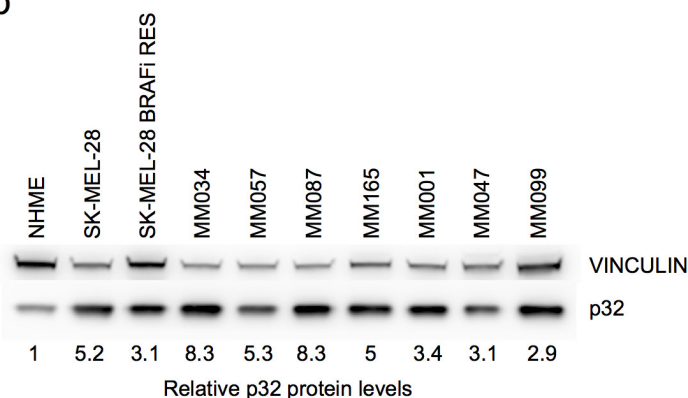


**Extended Data Figure 6 | A large fraction of cytoplasmic SAMMSON co-localizes with mitochondria. SAMMSON and mitochondrial 16S rRNA RNA-FISH in four different melanoma cell lines. SAMMSON probes, labelled with Quasar570, are shown in red and 16S rRNA probes, labelled with Quasar670, are shown in yellow; DAPI is in cyan.**

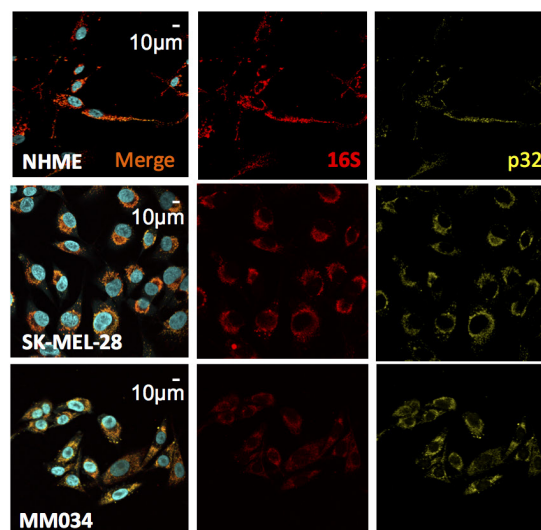
a

	PSMs	Peptide sequences	Protein IDs	FDR
<b>Control 1</b>	2043	1693	359	0.8%
<b>Control 2</b>	601	476	125	1.2%
<b>Control 3</b>	493	404	111	1.5%
<b>PD1</b>	482	376	101	1.7%
<b>PD2</b>	1097	747	151	1.1%
<b>PD3</b>	2719	2152	557	0.4%

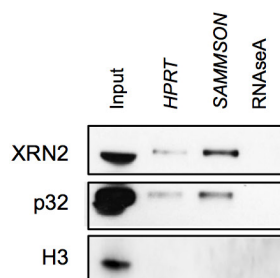
b



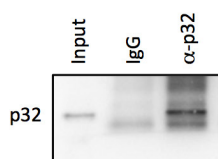
c



d

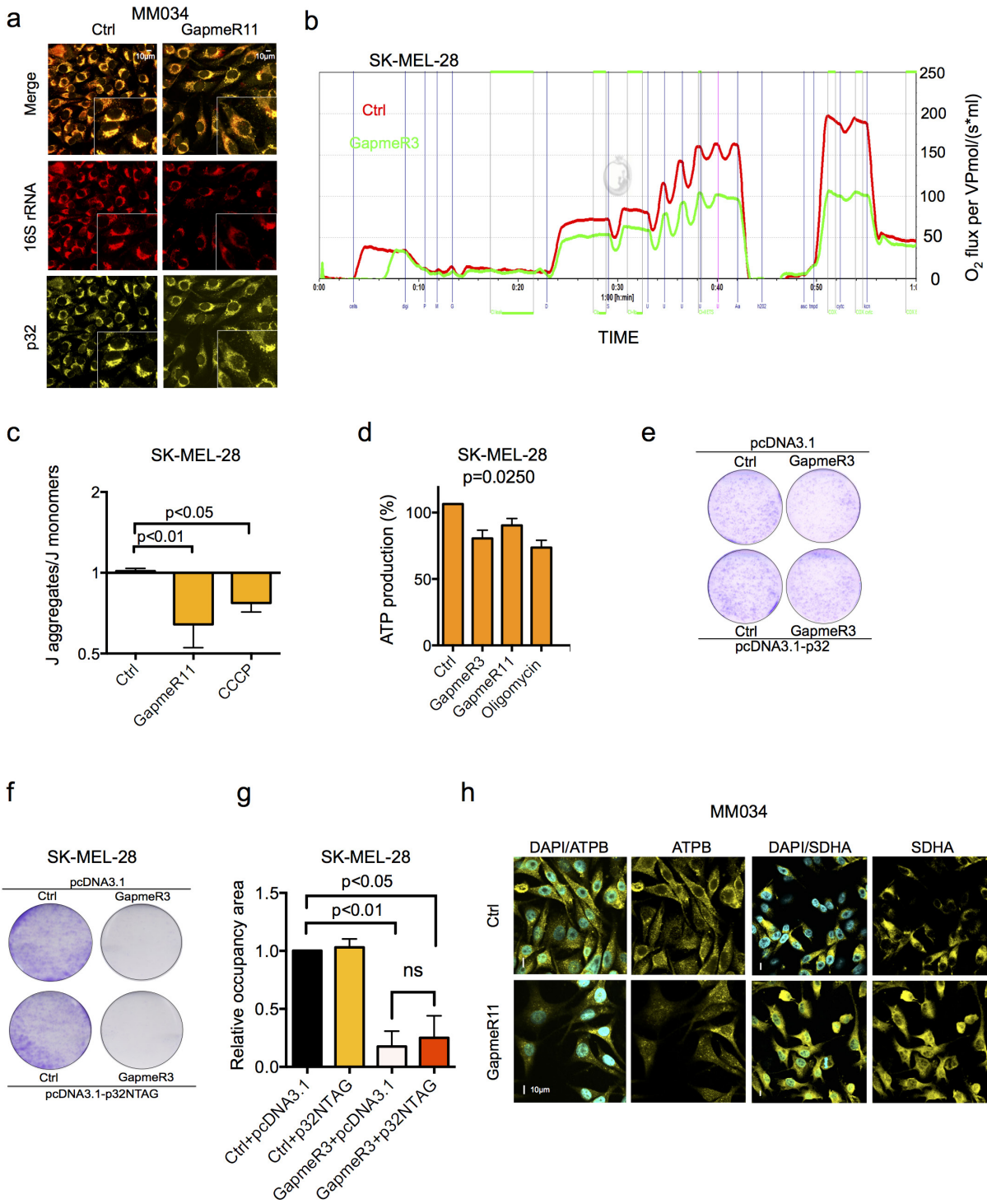


e



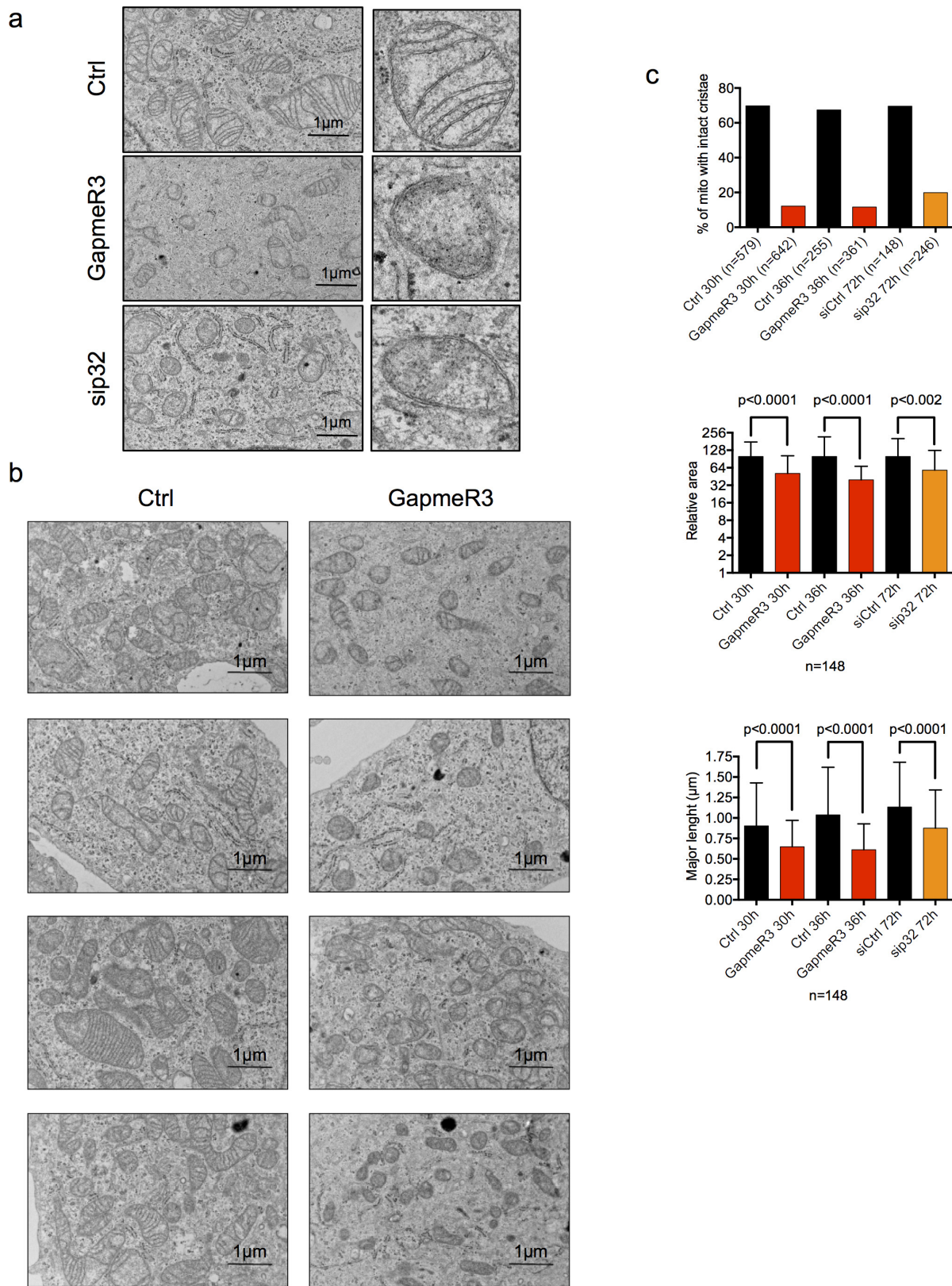
**Extended Data Figure 7 | RAP-MS identifies the mitochondrial protein p32 as a SAMMSON interactor.** **a**, The 'Metrics' table provides an overview of the MS experiment. For every MS analysis, the table contains the number of analysed spectra, the total number of identified spectra (peptide to spectra matches (PSMs)), the number of distinct peptide sequences, protein numbers and a false discovery rate (FDR) estimation based on searches against a reversed database. **b**, Western blot for p32 in NHMEs and in a panel of short-term melanoma cultures. Vinculin is

used as a loading control and normalizer for the quantification. **c**, RNA-FISH for 16S rRNA (in red) and immunofluorescence for p32 (in yellow) in NHMEs and in a panel of melanoma cell lines. DAPI is in cyan. **d**, Pull-down of SAMMSON (and HRPT) under native conditions and upon incubation with RNase A, followed by western blotting. **e**, Western blot confirming enrichment of p32 following immunoprecipitation with anti-p32 antibodies. **b**, **d**, **e**, For gel source data, see Supplementary Fig. 1.



**Extended Data Figure 8 | SAMMSON modulates mitochondrial metabolism in a p32-dependent manner.** **a**, RNA-FISH for 16S rRNA (in red) and immunofluorescence for p32 (in yellow) in melanoma cells (MM034) transfected with a control GapmeR (Ctrl) or with GapmeR11. Magnification,  $\times 200$ . **b**, Evaluation of OXPHOS complexes functionality by high-resolution respirometry in SK-MEL-28 treated with GapmeR3. The graph shows one representative experiment. **c**, JC-1 reveals a decrease in mitochondrial membrane potential upon GapmeR11 transfection, as assessed by the ratio between J-aggregates and J-monomers. The graph is an average of four different biological replicates  $\pm$  s.e.m. *P* values were calculated by ANOVA. **d**, Evaluation of ATP production in SK-MEL-28 transfected with GapmeRs and exposed to oligomycin (used here as control). ATP production measured by luciferase is expressed as a percentage, an average of three different experiments, relative to the

control sample (Ctrl)  $\pm$  s.e.m. *P* values were calculated by ANOVA. **e**, Colony formation assays 5 days after seeding SK-MEL-28 transfected with a control GapmeR (Ctrl) or GapmeR3, and either with an empty or a p32-expressing vector. **f**, Colony formation assays 5 days after seeding, showing cell growth of SK-MEL-28 transfected with a control GapmeR (Ctrl) or GapmeR3, and either with an empty vector or a vector expressing a tagged version of p32 that cannot localize to the mitochondria. **g**, Quantification of the colony assay described in **f**. The data represent the density (occupancy area) relative to the Ctrl + pcDNA3.1 sample. The data are presented as average of three different biological replicates  $\pm$  s.e.m. *P* values were calculated by ANOVA. **h**, Immunofluorescence using antibodies directed against SDHA and ATPB in MM034 melanoma cells upon GapmeR11 transfection. Magnification,  $\times 600$ .



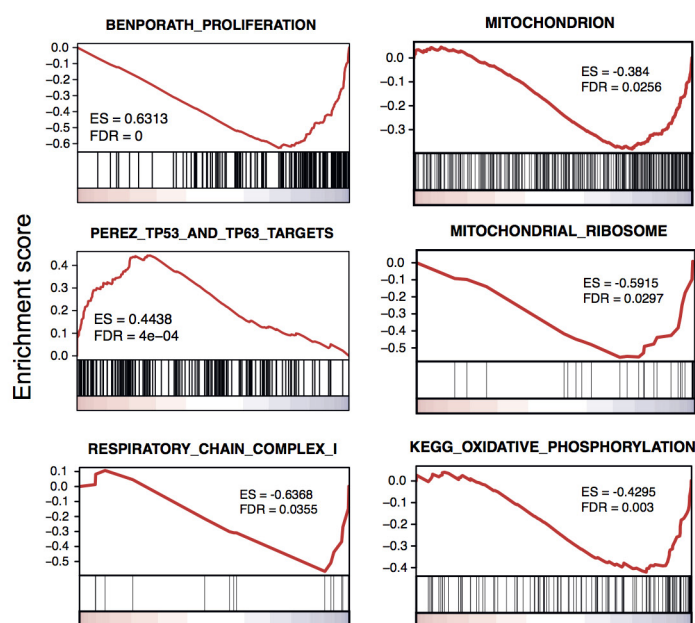
**Extended Data Figure 9 | SAMMSON and p32 silencing affects mitochondria integrity.** **a, b,** Representative electron microscopy images of melanoma cells transfected with Ctrl GapmeR and GapmeR3 or with siRNA targeting p32. **c,** Quantification of percentage of mitochondria

with intact cristae (top) and area and length (middle and bottom) in cells described in **b**; the total number of mitochondria evaluated per condition is indicated on the x-axis.

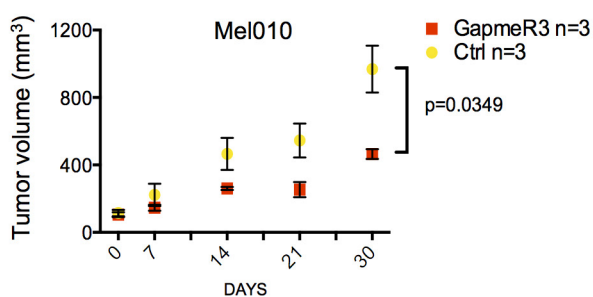
a

Patient	Mel006	Mel010
Gender	Female	Female
Year of birth	1947	1955
Biopsy origin	In transit metastasis	Lymph node
Biopsy site	Arm	Chest
Treatment prior to biopsy	none	none
BRAF V600 status	V600E	V600E
NRAS Q61 status	WT	WT
p53 status	WT (SNP c.215C>G; p.P72R)	WT (SNP c.215C>G;p.P72R)

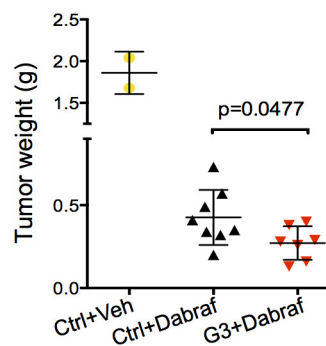
b



c



d



**Extended Data Figure 10 | SAMMSON silencing decreases melanoma growth *in vivo*.** a, Table describes the origin and *BRAF*, *NRAS* and *TP53* mutational status of the melanoma lesions that were used to generate the Mel006 and Mel010 PDX models. b, Gene set enrichment analyses among differentially expressed genes in melanoma lesions obtained from Mel006 PDX mice treated (i.v. injections) with a control GapmeR (Ctrl) or GapmeR3. c, Tumour volume of cohorts of Mel010 PDX mice treated

(intra-tumour injections) with a control GapmeR (Ctrl) or GapmeR3. Data are means  $\pm$  s.d. of three different biological replicates (*P* value was calculated by two-ways ANOVA). d, Tumour weight of the melanoma lesions derived from PDX mice (Mel006) treated with combinations of control GapmeR (Ctrl) and GapmeR3 with either vehicle or dabrafenib by daily oral gavage (vehicle or dabrafenib) and i.v. injection of the GapmeRs every 2 days. *P* value was calculated by *t*-test.